Au/TS-1 Catalyst for Propene Epoxidation with H2/O2: A Novel Strategy to Enhance Stability by Tuning Charging Sequence

Journal:	*AIChE Journal*
Manuscript ID	AIChE-15-17633.R1
Wiley - Manuscript type:	Research Article
Date Submitted by the Author:	n/a

Complete List of Authors:	Feng, Xiang; China University of Petroleum (huadong), State Key Laboratory of Heavy Oil Processing Liu, Yibin; China University of Petroleum Huadong - Qingdao Campus Li, Yichuan; China University of Petroleum (huadong), State Key Laboratory of Heavy Oil Processing Zhang, Zhihua; East China University of Science and Technology, State Key Laboratory of Chemical Engineering Duan, Xuezhi; East China University of Science and Technology, State Key Laboratory of Chemical Engineering Chen, De ; NTNU Zhou, Xinggui; East China University of Science and Technology, State Key Laboratory of Chemical Engineering Yang, Chaohe; China University of Petroleum, Department of Chemical Engineering

Keywords:	Propene epoxidation, deposition-precipitation method, charging sequence, Au location, catalytic stability

Au/TS-1 Catalyst for Propene Epoxidation with H_2/O_2: A Novel Strategy to Enhance Stability by Tuning Charging Sequence

Xiang Feng[a], Yibin Liu[a], Yichuan Li[a], Zhihua Zhang[b], Xuezhi Duan[b], De Chen[c], Xinggui Zhou[b,*] and Chaohe Yang[a,*]

[a] *State Key Laboratory of Heavy Oil Processing, China University of Petroleum (East China), Qingdao 266580, China.*

[b] *State Key Laboratory of Chemical Engineering, East China University of Science and Technology, 130 Meilong Road, Shanghai 200237, China.*

[c] *Department of Chemical Engineering, Norwegian University of Science and Technology, Trondheim 7491, Norway.*

Abstract: For propene epoxidation with H_2 and O_2, the catalytic performance of Au/TS-1 catalyst is extremely sensitive to preparation parameters of deposition-precipitation (DP) method. In this work, effect of charging sequence in DP process on catalyst structure and catalytic performance of Au/TS-1 catalyst is first investigated. For different charging sequences, the compositions of Au complexes (e.g., $[AuCl(OH)_3]^-$) and pore property of TS-1 (i.e., with or without H_2O pre-filling micropores) could affect the transfer of Au complexes into the micropores, resulting in different Au locations and thus significantly different catalytic performance. Notably, when TS-1 is first filled with H_2O and then mixed with Au complexes, the reduced Au/TS-1 catalyst could expose Au nanoparticles on the external surface of TS-1 and show high stability. The results provide direct evidence showing that micropore blocking is the deactivation mechanism. Based on the results, a simple strategy to design highly stable Au/Ti-based catalysts is developed.

Keywords: Propene epoxidation, deposition-precipitation method, charging sequence, Au location, catalytic stability

*Corresponding author. E-mail address: xgzhou@ecust.edu.cn; yangch@upc.edu.cn

Introduction

Propylene oxide (PO) as a versatile chemical intermediate is used to synthesize derivatives such as polyurethane foams and propylene glycol. Traditional chlorohydrin and hydroperoxidation processes to produce PO usually suffer from environmental or economical problems. Since Haruta et al. reported an alternative process for PO production (i.e., direct propene epoxidation with H_2 and O_2) using Au/TiO_2 catalysts,[1] this environmentally benign, sustainable and simple process has attracted immense research interests.[2, 3]

For direct propene epoxidation with H_2 and O_2, the synergy between Au nanoparticles and isolated Ti^{4+}-containing supports is indispensable for PO formation.[4-7] This is because H_2O_2 synthesized by H_2 and O_2 on Au nanoparticles must transfer to isolated Ti^{4+} sites nearby and form Ti-OOH intermediate which entails the subsequent epoxidation of propene to PO. Therefore, measures have been taken to improve the Au-Ti synergy in the past decades.[5, 8-10] Deposition-precipitation (DP) method is most widely used to enhance this Au-Ti interaction because Au nanoparticles can be selectively deposited near active Ti^{4+} sites rather than Si^{4+} sites by adjusting the pH of Au solution higher than the isoelectric point of the inactive Si^{4+} sites. To date, a series of Au/Ti-containing catalysts (e.g., Au/uncalcined TS-1, Au/TS-1, Au/Ti-HMS, Au/Ti-TUD, Au/three-dimensional Ti-Si mesoporous zeolite, $Au/Ti\text{-}SiO_2$) prepared by DP method are efficient for propene epoxidation.[6, 7, 11-26] Among others, Au/TS-1 catalyst shows superior catalytic performance due to the unique physico-chemical properties of TS-1 support (e.g., abundant isolated Ti^{4+} species and high hydrophobicity).[7]

The catalytic activity of Au catalyst is reported to be significantly affected by the preparation parameters of DP method.[11, 25-29] For instance, Louis et al. reported that thorough washing could reduce the concentration of chlorine ions, leading to smaller Au particle size and higher catalytic performance.[30] Delgass et al. found that preparation temperature affects the Au loading efficiency and Au particle size.[26] Higher temperature results in the aggregation of Au species via condensation reaction, and thus the poorer PO formation rate. Lu et al. found that the pH of Au solution could also affect Au loading efficiency, and pH of 7 is more appropriate for PO formation.[28] Zhou et al. elucidated that the effect of aging time on the Au particle size distribution and the catalytic performance.[31] Although much attention has already been focused on the preparation parameters, the Au/TS-1 catalysts under similar preparation conditions still show significantly different Au atom efficiencies ($g_{PO}h^{-1}kg_{Au}^{-1}$).[27, 28, 32] Therefore, in-depth investigation on the effects of preparation parameters on physico-chemical properties and performance of Au catalysts are highly desired not only to the explanation of different catalytic behaviors but also to the rational design of more effective Au/Ti-containing catalysts for direct propene epoxidation.

Besides activity, the catalytic stability is another essential criterion for efficient Au catalysts. For traditional Au/Ti-containing catalysts prepared by DP method, one common issue is the fast deactivation. We proposed that the deactivation is mainly caused by micropore blocking, and then employed a special support (i.e., uncalcined TS-1 with TPA^+ template inside the micropores) to deposit Au nanoparticles on the external surfaces of TS-1.[5, 6, 7,31] The as-obtained Au/uncalcined TS-1 catalyst shows as expected high stability. However, this methodology to enhance the catalytic stability may not be extended to some Ti-containing supports because the chemical properties of templates are distinct. Therefore, there is an urgent need to develop a simple strategy to

improve the catalytic stability of Au/Ti-containing catalyst.

Herein, for the first time, the effect of charging sequence on catalytic structure and performance of Au/TS-1 catalyst for propene epoxidation with H_2 and O_2 is examined by multi-techniques such as in-situ UV-vis, HAADF-STEM, XPS, TGA and N_2 physisorption. It is revealed that the different compositions of Au complexes and pore structure of TS-1 (i.e., with or without water molecules inside the micropores) for each charging sequence greatly affect the mass transfer, i.e., the entrance of Au complexes in the micropores. This leads to different Au locations and catalytic performances. Notably, when the TS-1 support is first prefilled with water molecules and then mixed with Au complexes, the reduced Au/TS-1 catalyst has Au nanoparticles located on the external surfaces of TS-1. The as-obtained Au/TS-1 catalyst shows high stability, which is found to be due to the absence of micropore blocking phenomenon. Moreover, an efficient method derived from the deactivation mechanism is further developed to enhance the catalytic stability of Au/TS-1 catalyst from experimental and theoretical aspects. The insights in this work not only elucidate the effect of charging sequence on Au location and catalytic performance, but also provide an efficient scenario to enhance the catalytic stability of Au/Ti-containing catalyst for propene epoxidation. It is expected that this strategy could be extended to other supported metal catalysts to avoid the deactivation caused by micropore blocking phenomenon.

Experimental

Synthesis of TS-1 support and Au/TS-1 catalysts

Titanium silicalite-1 (TS-1) support was synthesized by traditional hydrothermal method according to previously reported synthesis procedure.[26, 33] In a typical procedure,

3.5 g polyoxyethylene 20-sorbitan monolaurate (Tween 20, Aldrich) was added to 50 mL deionized water at room temperature. Subsequently, a mixture of 66.4 g tetraethylorthosilicate (TEOS, 95 wt%) and 44.8 g tetrapropylammonium hydroxide (TPAOH, 25 wt%) was slowly added to the above solution under vigorously stirring. Afterwards, the required titanium (IV) tetrabutoxide (TBOT, 99 wt%) dissolved in 20 mL isopropanol (WAKO, 99.5 wt%) was added drop-wise to achieve Si/Ti molar ratio of 100. The resultant solution was then transferred to a Teflon autoclave and crystallized at 423 K for 48 h. The solid products were filtered and thoroughly washed with deionized water. Finally, the solid (i.e., uncalcined TS-1) is dried overnight and calcined at 823 K for 6 h. The as-obtained material is microporous TS-1.

Au/TS-1 catalysts with Au loading of 0.10wt% were prepared by the deposition-precipitation (DP) method with three different charging sequences as follows:

(1) Sequence A: 0.1 g $HAuCl_4 \cdot 3H_2O$ and 40 mL H_2O were mixed for 30 min. Meanwhile, 0.5 g TS-1 was added to 10 mL H_2O. The pH values of the two mixtures were adjusted to 7.3-7.5 by 1 M NaOH, respectively. Finally, the two mixtures were blended together and aged for ca. 9 h while the pH was maintained constant by adding a small amount of NaOH. The solid was then centrifuged for 30 min, washed twice with deionized water and dried at 28 ^{o}C under vacuum. The as-prepared catalyst is denoted as Au/TS-1-SA.

(2) Sequence B[5-7, 26, 27]: 0.5 g TS-1, 0.1 g $HAuCl_4 \cdot 3H_2O$ and 50 mL H_2O were mixed together and stirred for 30 min. Afterwards, the pH of the slurry was adjusted to 7.3-7.5 by 1 M NaOH and then aged for ca. 9 h. The as-synthesized solid was centrifuged, washed with deionized water and then dried under vacuum at room temperature. The

catalyst is denoted as Au/TS-1-SB.

(3) Sequence C[28, 34]: 0.1 g $HAuCl_4 \cdot 3H_2O$ and 50 mL H_2O were mixed for 30 min. The pH of Au solution was adjusted to 7.3-7.5 by 1 M NaOH. Subsequently, 0.5 g TS-1 was added to the above Au solution and the pH of Au slurry was maintained for ca. 9 h. The solid was then centrifuged for 30 min, washed twice with deionic water and dried at 28 ^oC under vacuum at room temperature. The as-synthesized catalyst is denoted as Au/TS-1-SC.

Catalyst characterization

The crystal phase of TS-1 was characterized by X-ray diffraction (XRD, Rigaku D/Max2550VB/PC, Cu K_α radiation). The micropore volumes of TS-1 and Au/TS-1 samples were measured by N_2 physisorption in a volumetric adsorption unit (Micromeritics ASAP 2020). The local environment of titanium (e.g., isolated Ti^{4+}, anatase TiO_2) was determined by diffuse reflectance ultraviolet-visable spectroscopy (DRUV-vis, Perkin Elmer Lambda 35) and fourier transform infrared spectroscopy (FT-IR, Nicolet 6700). The types of Au complexes at different charging sequence and different time were determined by in situ ultraviolet-visable spectroscopy on a spectrometer (in situ UV-vis, AvaSpec-2048) equipped with a transmission dip probe. The contents of carbonaceous deposits at different time-on-steam were analyzed by thermogravimetric analysis (TGA, Perkin Elmer TGA Pyris 1). The TGA analysis was performed by heating approximate 10 mg of dried sample from room temperature to 800^oC at a ramping rate 5^oC/min in a flow of N_2/O_2=8:1. The Au loadings were determined by atomic absorption spectroscopy (AAS, ZEEnit 600). The surface Au/Si molar ratios were analyzed by X-ray photoelectron spectroscopy (XPS) on a Kratos XSAM-800 instrument. Al K_α X-ray of 1486.6 eV is used as the excitation source. The

chloride ion concentration was examined by ion chromatography (Dionex 600). The average particle size and particle size distribution are determined by high-angle annular dark-field scanning transmission electron microscopy (HAADF-STEM) on a Tecnai G2 F20 S-Twin equipped with a digitally processed STEM imaging system. The Au particle size distribution was determined by measuring more than 150 nanoparticles.

Catalytic testing

Gas-phase propene epoxidation over Au/TS-1 catalysts was carried out at normal pressure in a feed gas mixture of C_3H_6: H_2: O_2: N_2 =1:1:1:7 at a space velocity of 14,000 $mLh^{-1}g_{cat}^{-1}$ under atmospheric pressure. 0.15 g catalyst of 60-80 mesh particle size was packed in a quartz tubular reactor (i.d. 8 mm). The reactor was heated from room temperature to 200 ^oC for reaction. The effluent was measured online by two gas chromatographs (Agilent 6890) equipped with TCD (Porapak Q and 5A columns) and FID (Porapak T column) detectors. The propene conversion, PO selectivity and H_2 selectivity were defined as follows:

Propylene conversion = mol of (C_3-oxygenates + 2/3ethanal + CO_2/3)/mol of propene in the feed.

PO selectivity = mol of PO/mol of (C_3-oxygenates + 2/3ethanal + CO_2/3).

H_2 selectivity = mole of PO/mol of H_2 converted.

Results and discussion

Effect of charging sequence

The charging sequence of deposition-precipitation process is easily overlooked. There is still no report on the effect of charging sequence on the physico-chemical structure of

catalyst and catalytic performance for propene epoxidation. It should be noted that when the charging sequence varies, the interaction between Au complexes and support may be different, which could result in different catalytic structure and performance.

The compositions of Au complexes for each charging sequence are investigated by UV-vis spectroscopy. Figure 1 shows the UV-vis spectrum of Au solution at different pH values. It can be seen that two adsorption bands ascribed to the ligand-to-metal charge transfer (LMCT) transitions from chlorine *p* to gold *d* orbitals are located at ca. 240 and 313 nm, which are associated with $p_\sigma \rightarrow d_{x^2-y^2}$ and $p_\pi \rightarrow d_{x^2-y^2}$ transitions, respectively.[35, 36] When the pH value is higher, the adsorption bands are blueshifted and the band intensities are gradually reduced. The reason for the change of bands is the hydrolysis of Au complexes, i.e., the gradual replacement of chloride by hydroxyl ions.[37] Table S1 shows the compositions of Au complexes at different pH values according to the literature.[38, 39] For example, the composition of Au complexes changes from $[AuCl_4]^-$ and $[AuCl_3(OH)]^-$ gradually to $[AuCl_2(OH)_2]^-$, $[AuCl(OH)_3]^-$ and $[Au(OH)_4]^-$ when the pH increases from 2 to 7. Based on the compositions of Au complexes at different pH values (Table S1) and the corresponding UV-vis spectra at different pH (Figure 1), it is therefore feasible to determine the compositions of Au complexes at each charging sequence from in-situ UV-vis spectra. Figure 1 also shows the in-situ UV-vis spectra of Au complexes for three charging sequences when TS-1 is mixed with Au solution. For charging sequence A and C, the pH of Au solution is already adjusted to 7.3-7.5 when TS-1 is added. There is only one adsorption band for Au/TS-1-SA and Au/TS-1-SC locating between the two bands at pH of 6 and 7. This indicates that the hydrolysis equilibrium is not reached and the composition of Au complexes should be $[AuCl_2(OH)_2]^-$, $[AuCl(OH)_3]^-$ and $[Au(OH)_4]^-$. For charging

sequence B, the pH value is still 2.3 when TS-1 is added, and the Au complexes are $[AuCl_4]^-$ and $[AuCl_3(OH)]^-$. The sizes of different Au complexes calculated by quench molecular dynamics[6] are shown in Table 1. It is clear that the size and steric hindrance of Au complexes with more chloride ions are larger. In addition, the sizes and steric hindrance of Au complexes for charging sequence B are larger than those for charging sequence A and C. Notably, the sizes of Au complexes are similar to the diameter of micropore, and Au complexes could enter into the micropores by stretching and bending vibrations but with difficulties.[31]

(Figure 1 should be inserted here)

(Table 1 should be inserted here)

TS-1 is employed as support to load the above Au complexes. Figure 2a shows the typical X-ray power diffraction pattern of TS-1 and the reference material of silicate-1. The two samples are high crystalline with the absence of an amorphous phase. It is clear that different diffraction peaks are located at $2\theta=7.9^o$, 8.8^o, 23.1^o, 23.9^o and 24.3^o, indicating the characteristic of MFI topological structure.[40] There is a single peak at $2\theta=24.3^o$ for TS-1, indicating the structure of orthorhombic unit cell symmetry.[26] This is obviously different from the two peaks at $2\theta=24.3^o$ for silicate-1, which is the characteristic of monoclinic unit cell symmetry. In addition, the peak ascribed to crystalline TiO_2 in the form of anatase at $2\theta=25.4^o$ is not observed for the TS-1 sample.[34] Figure 2b illustrates the nitrogen adsorption-desorption isotherms and pore size distribution of the TS-1 sample. According to the IUPAC classification, TS-1 exhibits typical type I isotherm with a steep rise at low relative pressure $P/P_0<0.01$, confirming the microporous character. The pore size distribution is determined by NL-DFT method, which shows accurate pore size distribution over the complete

micro/mesopore range. There is only a narrow peak centered at ca. 0.55 nm, fitting very well with the mean pore size of MFI structure.[7]

(Figure 2 should be inserted here)

Figure 3a shows the FT-IR spectrum of TS-1 sample. In accordance with XRD results, the MFI structure is certified by the band at 550 cm^{-1} which is assigned to the vibration of double five-membered ring unit.[31] The adsorption bands at 800 and 1100 cm^{-1} are attributed to the symmetrical and antisymmetrical stretching vibration of [SiO_4] units, respectively. In addition, the band at 1230 cm^{-1} is due to the asymmetrical stretching vibration of MFI framework structure. The peak at 960 cm^{-1} is often referred to Ti-O-Si band and is usually considered as a proof of Ti substitution into the framework.[41, 42] Figure 3b shows the UV-vis spectrum of TS-1. The dominant band centered at 210 nm is assigned to the $Ti^{4+}O^{2-}$ to $Ti^{3+}O^{-}$ ligand-to-metal charge transfer, and is characteristic of isolated tetrahedrally coordinated Ti atoms in framework.[43] No adsorption bands attributed to octahedrally coordinated Ti containing Ti-O-Ti bond or isolated Ti species coordinated water molecules[44] are observed at 240-290 nm. In addition, there is no adsorption band at 330 nm, indicating the absence of extra framework anatase TiO_2.[40] This is in consistant with the XRD results (Figure 2a).

(Figure 3 should be inserted here)

Table 2 shows the structural properties of TS-1 and Au/TS-1 samples. The micropore volume of pure TS-1 support is 0.16 $cm^3 \cdot g^{-1}$. After the deposition of Au clusters, the micropore volumes of Au/TS-1-SB and Au/TS-1-SC catalysts decrease from 0.16 to 0.13 and 0.11 $cm^3 \cdot g^{-1}$, respectively. The reduced micropore volume of Au/TS-1-SC catalyst (i.e., 0.05 $cm^3 \cdot g^{-1}$) is larger than that of Au/TS-1-SB catalyst (0.03

$cm^3 \cdot g^{-1}$), demonstrating that more Au clusters have entered into the microporous channels of TS-1. In contrast, the micropore volume of Au/TS-1-SA catalyst (0.16 $cm^3 \cdot g^{-1}$) is the same to that of pure TS-1 support. This indicates that Au nanoparticles do not enter the micropores but locate on the external surfaces of TS-1 for Au/TS-1-SA catalyst.

(Table 2 should be inserted here)

XPS is a powerful tool to analyze the surface composition of catalysts.[45] Table 3 shows the bulk and surface compositions of Au/uncalcined TS-1 and Au/TS-1 samples prepared with different charging sequences. The Au loadings of the four samples are carefully tuned to the same of 0.10 wt% in order to exclude the effect of Au loading on the XPS results. For the three Au/TS-1 catalysts, the bulk Au/Si molar ratios are quite similar due to the same Au loading. The surface Au/Si molar ratios are larger than bulk Au/Si molar ratios, confirming that Au nanoparticles tend to locate on the external surfaces of TS-1 rather than homogeneously distributed in the entire TS-1 volume.[11] In addition, the surface Au/Si molar ratios decrease in order of Au/TS-1-SA> Au/TS-1-SB> Au/TS-1-SC. This trend shows that more Au clusters are located inside the micropores for Au/TS-1-SC catalyst, in accordance with the N_2 physisorption results (i.e., minimum micropore volume of Au/TS-1-SC) in Table 2. Moreover, it can also be seen from Table 3 that the surface Au/Si molar ratios of Au/TS-1-SA and Au/uncalcined TS-1 catalysts are almost the same. For Au/uncalcined TS-1 catalyst, Au nanoparticles are deposited on the external surfaces of TS-1[7] because the TPA^+ template already blocks the micropores. This similar surface Au/Si molar ratios of Au/TS-1-SA and Au/uncalcined TS-1 catalysts corroborates that almost all the Au nanoparticles of Au/TS-1-SA catalyst are deposited on the external surfaces of microporous TS-1.

(Table 3 should be inserted here)

Figure 4 shows the typical HAADF-STEM images and particle size distributions of Au/TS-1 catalysts prepared with different charging sequences. The observable average Au particle size of the three samples are quite similar (Figure 4). However, the number of observable Au nanoparticles on the external surfaces of TS-1 decreases in order of Au/TS-1-SA> Au/TS-1-SB> Au/TS-1-SC. This tendency indicates that more Au nanoparticles are deposited on the external surface of TS-1 for Au/TS-1-SA catalyst while more Au clusters are located inside the micropores of Au/TS-1-SC catalyst. This indirect evidence is also in accordance with N_2 adsorption and XPS results.

(Figure 4 should be inserted here)

The unique location of Au nanoparticles on external surfaces of Au/TS-1-SA catalyst can be explained by the work of Gavriilidis.[46] They reported that when the support is dry, the solution can fill the pores of support and initially convective transport takes place.[46] However, when the support is wet with pure H_2O molecules (ca. 0.5 nm[47]) filling the pores, no convective solute transport takes place in the pores. Therefore, there is no more chemical reaction between Au complexes and Ti-OH inside the micropores. Subsequently, the hydrolyzed Au complexes in the solution react with Ti-OH groups on the external surfaces and pore mouth of TS-1 support (i.e., interface between pure H_2O inside micropores and Au complexes outside micropores). The as-formed hydroxy-gold species in the pore mouth may suppress the further diffusion of Au complexes into the micropores. This may be the reason for the unique Au location on Au/TS-1-SA catalyst. With respect to the more Au complexes inside the micropores of Au/TS-1-SC than Au/TS-1-SA catalyst, it is mainly because the size and steric hindrance of Au complexes for Au/TS-1-SC is smaller than that of Au/TS-1-SA catalyst when TS-1 is charged

(Table 1).

Figure 5 shows the different catalytic performances of three Au/TS-1 catalysts. PO formation rate and selectivity were determined at time-on-steam of 1h at 200°C. The PO selectivity of the three catalysts are ca. 90% and the selectivity of side products such as acetone, ethanal, propanal, carbon dioxide are also similar. The hydrogen efficiency of the Au/TS-1-SC catalyst is 22%, slightly higher than that of Au/TS-1-SA (18%) and Au/TS-1-SB (15%) catalysts. The slightly higher hydrogen efficiency of the Au/TS-1-SC catalyst is mainly because it contains more tiny Au nanoparticles inside microporous channels of TS-1 support. This part of tiny Au nanoparticles usually exhibit higher H_2 efficiency due to smaller Au particle size.[6] The PO formation rate of the three catalysts are obviously different, as shown in figure 5b. The differences are not due to effect of chloride because the careful washing eliminates chloride ions, as evidenced by the results of ion chromatography (Table S2). For 0.10 wt% Au/TS-1-SC catalyst, the initial PO formation rate is 185 $g_{POh}^{-1}g_{Au}^{-1}$, which is the highest among the three catalysts. For 0.10 wt% Au/TS-1-SB catalyst, the initial PO formation is slightly smaller than that of Au/TS-1-SC catalyst. It is reported by Delgass et al. that Au clusters inside the micropores may serve as the dominant active sites.[25] This statement is also supported by our previous works.[5-7, 31] Therefore, the higher initial PO formation rate for Au/TS-1-SC catalyst than Au/TS-1-SB catalyst is mainly due to larger proportion of Au clusters inside micropores of TS-1. Compared with Au/TS-1-SB and Au/TS-1-SC catalysts, the initial PO formation rate of Au/TS-1-SA catalyst is smaller. This may be due to the absence of the contribution of small quantity of high active Au clusters inside micropores of TS-1. Although the initial catalytic activity of Au/TS-1-SA catalyst is slightly lower than that of Au/TS-1-SB and Au/TS-1-SC catalysts, it shows high stability and thus higher stable catalytic activity after 20 h. This finding is also in

consistent with our previous finding[31] that with less Au clusters inside micropores of TS-1 support, the Au/TS-1 catalyst shows higher stable activity. The effect of charging sequence on Au locations and catalytic performance is shown in Figure 6.

(Figure 5 should be inserted here)

(Figure 6 should be inserted here)

New method to improve the catalytic stability

Fast deactivation is one of the key factors hindering the industrialization of Au/Ti-based catalysts. The Au/TS-1-SB and Au/TS-1-SC catalysts all suffer from the severe deactivation although the catalytic activities are high (Figure 5). In our previous work, we deposited Au nanoparticles on the external surfaces of uncalcined TS-1 which has TPA^+ template inside the micropores. The designed Au/uncalcined TS-1 catalyst shows significantly enhanced stability because of the easy transfer of reactants and products on the external surfaces of TS-1. However, the enhanced stability may also be attributed to the presence of amine species. In other words, the contribution of amine species generated during external TPA^+ decomposition on catalytic stability cannot be excluded. Herein, the Au/TS-1-SA catalyst is employed to elucidate the origin of the enhanced stability because Au/TS-1-SA catalyst does not contain any TPA^+ template.

The origin of the different catalytic stabilities of Au/TS-1-SA and Au/TS-1-SB catalysts is investigated by analyzing the volume of carbonaceous deposits (V_c) and the volume not accessible to N_2 molecules (V_{na}).[48-50] This analysis could show the relationship between carbonaceous deposits and TS-1 support (i.e., pore blocking and pore filling, as illustrated in Figure 7a). When carbonaceous deposits only lead to micropore filling, V_c should be equal to V_{na} and thus V_c/V_{na}=1. In contrast, V_c should be

smaller than V_{na} when the carbonaceous deposits cause micropore blocking, and hence V_c/V_{na}<1. When the carbonaceous deposits mainly block the pore mouth, V_c should be much smaller than V_{na}. The V_c is calculated by dividing the weight of carbonaceous deposits (i.e., w_c) by density of carbonaceous deposits (i.e., ρ_c), which are determined by TGA and FT-IR, respectively. The density of carbonaceous deposits with aromatic character (Figure S1) is usually 1.2 g·cm^{-3}.[50] Figure 7b shows the V_c/V_{na} of Au/TS-1-SA and Au/TS-1-SB catalysts as a function of time-on-steam. The values of V_c and V_{na} for Au/TS-1-SA and Au/TS-1-SB catalysts are summarized in Table 4. The data of Au/TS-1-SA is taken from our previous work.[7] It can be seen that V_c/V_{na} of Au/TS-1-SA catalyst decreases sharply from 1.00 to 0.75 in 20 h, indicating that micropore blocking is the deactivation mechanism. However, with the increase of volume of carbonaceous deposits, the volume not accessible to N_2 molecules (V_{na}) is slightly unchanged for Au/TS-1-SA catalyst (Table 4). This may be because carbonaceous deposits formed near Au nanoparticles on the external surface of TS-1 do not greatly affect the micropore volume. Consequently, the increasing V_c and almost unchanged V_{na} leads to large V_c/V_{na} of ca. 2.5 (larger than 1.0). The results demonstrate that micropore blocking phenomenon on Au/TS-1-SB catalyst does not occur on Au/TS-1-SA catalyst. Besides micropore blocking, another deactivation mechanism for Au catalysts is usually the Au aggregation. However, obvious Au aggregation is not observed for Au/TS-1 catalysts in propene epoxidation, as shown in Figure S2. This is also supported by other researchers.[7, 20, 28] Therefore, the origin for the high stability of Au/TS-1-SA catalyst is the unique location of Au on the external surfaces of TS-1 and hence the absence of micropore blocking phenomenon. When micropore blocking occurs, it is thus difficult for reactants and products to transfer into and out of the micropores of Au/TS-1-SB, inhibiting the reaction on internal Au-Ti active sites. Nevertheless, the easy mass

transfer on the external surfaces of Au/TS-1-SA guarantees the smooth epoxidation reaction.

(Figure 7 should be inserted here)

(Table 4 should be inserted here)

Without the TPA template, it is also feasible to deposit Au nanoparticles on the externals surfaces of TS-1 by manipulating the charging sequence. Figure 8 shows the catalytic performance of a series of Au/TS-1 catalysts prepared with charging sequence A in the initial 15 h. It is clear that none of the Au catalysts show any sign of deactivation, indicating that depositing Au nanoparticles on the external surfaces of support could indeed enhance the stability due to better mass transfer. With the increase of Au loading, the PO formation rate monotonously increases from 105 to 153 $g_{PO}h^{-1}kg_{Cat}^{-1}$. It should be noted that the normalized reaction rate ($g_{PO}h^{-1}g_{Au}^{-1}$) of 0.15Au/TS-1-SA catalyst is slightly lower than that of 0.08Au/TS-1-SA catalyst due to larger Au average particle size. Synthesizing smaller Au nanoclusters with high loading should be an effective approach to further enhance the catalytic activity, which will be carried out in our future research.

(Figure 8 should be inserted here)

The PO formation rate of reported stable Au/Ti-based catalysts without adding promoters are summarized in Table 5. The four Au catalysts including Au/TS-1-SA in this work all show Au nanoparticles on the external surfaces of TS-1 supports. The first two Au catalysts prepared by sol-immobilization (SI) and solid-grinding (SG) methods are effective for PO production, especially when promoters (e.g., ionic liquid and

alkaline) are added.[3, 21] In comparison, the Au/uncalcined TS-1 and Au/TS-1-SA catalysts prepared by DP method show much higher catalytic performance. This is mainly because Au nanoparticles could be selectively deposited near the Ti^{4+} sites rather than Si^{4+} sites by tuning the pH of solution higher than isoelectric point of Si^{4+} sites, which enhances Au-Ti synergy. With respect to the PO selectivity, the Au/TS-1-SA catalyst in this work is better than Au/uncalcined TS-1 catalyst. This is possibly due to the smaller Au particle size (Figure 4). The optimized catalytic performance of Au/TS-1-SA catalyst (i.e., 153 $g_{PO}h^{-1}kg_{Cat}^{-1}$) is already comparable to that of ethylene epoxidation to ethylene oxide (i.e., 134 $g_{PO}h^{-1}kg_{Cat}^{-1}$) in commercial plants.[51] The H_2 efficiency of Au/TS-1-SA catalyst can be further improved by reducing Si/Ti molar ratio of support since lower Si/Ti ratio favors the capture of H_2O_2 by the titanium centers near Au nanoparticles, thus hindering the direct decomposition of H_2O_2 to H_2O.[5] For zeolite catalyzed reactions (e.g., direct propene epoxidation with H_2 and O_2), a phenomenon is that reactants and products may face severe diffusion limitations that often lead to rapid catalyst deactivation by coke formation which blocks the pores. For propene epoxidation, if microporous materials supported Au catalysts (e.g., Au/Ti-MWW, Au/Ti-β, Au/TS-2) suffer from deactivation by micropore blocking, this strategy to deposit Au nanoparticles on the external surfaces may provide a promising way to enhance catalytic stability.

(Table 5 should be inserted here)

Conclusions

In this work, the effects of charging sequence in DP process on the structure and catalytic performance of Au/TS-1 catalyst are first investigated. It is found that the

composition of Au complexes and pore structure of TS-1 support (i.e., with or without H_2O molecules pre-filling the micropores) could affect the ability of Au complexes transferring into the micropores of TS-1, and thus change Au locations on the internal or external surfaces of support after reduction. When dry TS-1 support is mixed with small-sized Au complexes, more Au complexes could enter into the microporous channels of TS-1, resulting in higher initial PO formation rate but fast deactivation caused by micropore blocking. However, when TS-1 is first filled with H_2O and then mixed with Au complexes, the Au complexes are located on the external surfaces of TS-1 support. Consequently, the catalyst shows greatly enhanced stability. The reason for the stability is the absence of micropore blocking phenomenon as evidenced by the large V_c/V_{na} of used Au/TS-1-SA catalyst. Moreover, based on this strategy to enhance the catalytic stability using the charging sequence A, the 0.15wt% Au/TS-1-SA catalyst shows not only good stability over 15 h but also high PO formation rate of 153 $g_{PO}h^{-1}kg_{Cat}^{-1}$. This strategy is of referential importance to the design of highly stable Au/Ti-based catalysts for propene epoxidation with H_2 and O_2. It is hoped that this method could also be employed to enhance catalytic stability of other industrial supported metal catalysts that suffers from micropore blocking deactivation.

Acknowledgments

This work is financially supported by the 111 Project of Ministry of Education of China (B08021), China Postdoctoral Science Foundation (2015M582160) and the Open Project of State Key Laboratory of Chemical Engineering (SKL-ChE-15C04).

References

1 Haruta M, Uphade BS, Tsubota S, Miyamoto A. Selective oxidation of propylene

over gold deposited on titanium-based oxides. *Res Chem Intermed.* 1998;24:329-336.

2 Hayashi T, Tanaka K, Haruta M. Selective Vapor-Phase Epoxidation of Propylene over Au/TiO_2 Catalysts in the Presence of Oxygen and Hydrogen. *J Catal.* 1998;178:566-575.

3 Huang J, Takei T, Akita T, Ohashi H, Haruta M. Gold clusters supported on alkaline treated TS-1 for highly efficient propene epoxidation with O_2 and H_2. *Appl Catal B Environ.* 2010;95:430-438.

4 Bravo-Suarez JJ, Bando KK, Lu J, Haruta M, Fujitani T, Oyama T. Transient technique for identification of true reaction intermediates: Hydroperoxide species in propylene epoxidation on gold/titanosilicate catalysts by X-ray absorption fine structure spectroscopy. *J Phys Chem C.* 2008;112:1115-1123.

5 Feng X, Duan X, Yang J, Qian G, Zhou X, Chen D, Yuan W. Au/uncalcined TS-1 catalysts for direct propene epoxidation with H_2 and O_2: Effects of Si/Ti molar ratio and Au loading. *Chem Eng J.* 2014;278:234-239.

6 Feng X, Duan X, Qian G, Zhou X, Chen D, Yuan W. Insights into size-dependent activity and active sites of Au nanoparticles supported on TS-1 for propene epoxidation with H_2 and O_2. *J Catal.* 2014;317:99-104.

7 Feng X, Duan X, Qian G, Zhou X, Chen D, Yuan W. Au nanoparticles deposited on the external surfaces of TS-1: Enhanced stability and activity for direct propylene epoxidation with H_2 and O_2. *Appl Catal B Environ.* 2014;150:396-401.

8 Chen J, Halin SJ, Pidko EA, Verhoeven M, Ferrandez DMP, Hensen EJ, Schouten JC, Nijhuis TA. Enhancement of catalyst performance in the direct propene epoxidation: A study into gold-titanium synergy. *ChemCatChem.* 2013;5:467-478.

9 Qi C, Huang J, Bao S, Su H, Akita T, Haruta M. Switching of reactions between hydrogenation and epoxidation of propene over Au/Ti-based oxides in the presence of H_2 and O_2. *J Catal.* 2011;281:12-20.

10 Lee WS, Zhang R, Akatay MC, Baertsch CD, Stach EA, Ribeiro FH, Delgass WN. Differences in catalytic sites for CO oxidation and propylene epoxidation on Au nanoparticles. *ACS Catal.* 2011;1:1327-1330.

11 Lee W-S, Cem Akatay M, Stach EA, Ribeiro FH, Delgass WN. Enhanced reaction rate for gas-phase epoxidation of propylene using H_2 and O_2 by Cs promotion of Au/TS-1. *J Catal.* 2013;308:98-113.

12 Xu L, Ren Y, Wu H, Liu Y, Wang Z, Zhang Y, Xu J, Peng H, Wu P. Core/shell-structured TS-1@mesoporous silica-supported Au nanoparticles for selective epoxidation of propylene with H_2 and O_2. *J Mater Chem.* 2011;21:10852-10858.

13 Yang H, Tang D, Lu X, Yuan Y. Superior performance of gold supported on titanium-containing hexagonal mesoporous molecular sieves for gas-phase epoxidation of propylene with use of H_2 and O_2. *J Phys Chem C.* 2009;113:8186-8193.

14 Lu J, Zhang X, Bravo-Suárez JJ, Bando KK, Fujitani T, Oyama ST. Direct

propylene epoxidation over barium-promoted Au/Ti-TUD catalysts with H_2 and O_2: Effect of Au particle size. *J Catal.* 2007;250:350-359.

15 Qian G, Yuan YH, Wu W, Zhou XG, Vapor phase propylene epoxidation kinetics, *Stud Surf Sci Catal*. 2006;159:333-336.

16 Yuan YH, Zhou XG, Wu W, Zhang YR, Yuan WK, Luo L. Propylene epoxidation in a microreactor with electric heating. *Catal Today.* 2005;105:544-550.

17 Sinha AK, Seelan S, Akita T, Tsubota S, Haruta M. Vapor phase propylene epoxidation over Au/Ti-MCM-41 catalysts prepared by different Ti incorporation modes. *Appl Catal A Gen.* 2003;240:243-252.

18 Uphade BS, Akita T, Nakamura T, Haruta M. Vapor-phase epoxidation of propene using H_2 and O_2 over Au/Ti-MCM-48. *J Catal.* 2002;209:331-340.

19 Mul G, Zwijnenburg A, van der Linden B, Makkee M, Moulijn JA. Stability and selectivity of Au/TiO_2 and Au/TiO_2/SiO_2 catalysts in propene epoxidation: An in Situ FT-IR Study. *J Catal.* 2001;201:128-137.

20 Nijhuis TA, Huizinga BJ, Makkee M, Moulijn JA. Direct epoxidation of propene using gold dispersed on TS-1 and other titanium-containing supports. *Ind Eng Chem Res.* 1999;38:884-891.

21 Du M, Zhan G, Yang X, Wang H, Lin W, Zhou Y, Zhu J, Lin L, Huang J, Sun D, Jia L, Li Q. Ionic liquid-enhanced immobilization of biosynthesized Au nanoparticles on TS-1 toward efficient catalysts for propylene epoxidation. *J Catal.*

2011;283:192-201.

22 Sinha AK, Seelan S, Tsubota S, Haruta M. A three-dimensional mesoporous titanosilicate support for gold nanoparticles: Vapor-phase epoxidation of propene with high conversion. *Angew Chem Int Ed.* 2004;43:1546-1548.

23 Lee W-S, Cem Akatay M, Stach EA, Ribeiro FH, Nicholas Delgass W. Gas-phase epoxidation of propylene in the presence of H_2 and O_2 over small gold ensembles in uncalcined TS-1. *J Catal.* 2014;313:104-112.

24 Chen J, Pidko EA, Ordomsky VV, Verhoeven T, Hensen EJ, Schouten JC, Nijhuis TA. How metallic is gold in the direct epoxidation of propene: an FTIR study. *Catal Sci Tech.* 2013;3:3042-3055.

25 Lee WS, Lai LC, Cem Akatay M, Stach EA, Ribeiro FH, Delgass WN. Probing the gold active sites in Au/TS-1 for gas-phase epoxidation of propylene in the presence of hydrogen and oxygen. *J Catal.* 2012;296:31-42.

26 Lee WS, Cem Akatay M, Stach EA, Ribeiro FH, Delgass WN. Reproducible preparation of Au/TS-1 with high reaction rate for gas phase epoxidation of propylene. *J Catal.* 2012;287:178-189.

27 Huang J, Lima E, Akita T, Guzmán A, Qi C, Takei T, Haruta M. Propene epoxidation with O_2 and H_2: Identification of the most active gold clusters. *J Catal.* 2011;278:8-15.

28 Lu J, Zhang X, Bravo-Suárez JJ, Fujitani T, Oyama ST. Effect of composition and

promoters in Au/TS-1 catalysts for direct propylene epoxidation using H_2 and O_2. *Catal Today.* 2009;147:186-195.

29 Taylor B, Lauterbach J, Delgass WN. Gas-phase epoxidation of propylene over small gold ensembles on TS-1. *Appl Catal A Gen.* 2005;291:188-198.

30 Hugon A, El Kolli N, Louis C. Advances in the preparation of supported gold catalysts: Mechanism of deposition, simplification of the procedures and relevance of the elimination of chlorine. *J Catal.* 2010;274:239-250.

31 Feng X, Duan X, Cheng H, Qian G, Chen D, Yuan W, Zhou X. Au/TS-1 catalyst prepared by deposition-precipitation method for propene epoxidation with H_2/O_2: Insights into the effects of slurry aging time and Si/Ti molar ratio. *J Catal.* 2015;325:128-135.

32 Liu T, Hacarlioglu P, Oyama ST, Luo MF, Pan XR, Lu JQ. Enhanced reactivity of direct propylene epoxidation with H_2 and O_2 over Ge-modified Au/TS-1 catalysts. *J Catal.* 2009;267:202-206.

33 Khomane RB, Kulkarni BD, Paraskar A, Sainkar SR. Synthesis, characterization and catalytic performance of titanium silicalite-1 prepared in micellar media. *Mater Chem Phys.* 2002;76:99-103.

34 Sanz R, Serrano D, Pizarro P, Moreno I. Hierarchical TS-1 zeolite synthesized from SiO_2-TiO_2 xerogels imprinted with silanized protozeolitic units. *Chem Eng J.* 2011;171:1428-1438.

35 Gangopadhayay AK, Chakravorty A. Charge transfer spectra of some gold (III) complexes. *J Chem Phys.* 2004;35:2206-2209.

36 Peck JA, Tait CD, Swanson BI, Brown Jr GE. Speciation of aqueous gold (III) chlorides from ultraviolet/visible absorption and Raman/resonance Raman spectroscopies. *Geochim Cosmochim AC.* 1991;55:671-676.

37 Baatz C, Decker N, Prüße U. New innovative gold catalysts prepared by an improved incipient wetness method. *J Catal.* 2008;258:165-169.

38 Moreau F, Bond GC. Preparation and reactivation of Au/TiO_2 catalysts. *Catal Today.* 2007;122:260-265.

39 Nechayev YA, Nikolenko N. Adsorption of gold (III) chloride complexes on alumina, silica and kaolin. *Geochem Int.* 1986;23:142-146.

40 Duprey E, Beaunier P, Springuel-Huet M-A, Bozon-Verduraz F, Fraissard J, Manoli J-M, Brégeault J-M. Characterization of catalysts based on titanium silicalite, TS-1, by physicochemical techniques. *J Catal.* 1997;165:22-32.

41 Tatsumi T, Jappar N. Ammoximation of cyclic ketones on TS-1 and amorphous SiO_2-TiO_2. *J Catal.* 1996;161:570-576.

42 Zecchina A, Bordiga S, Lamberti C, Ricchiardi G, Scarano D, Petrini G, Leofanti G, Mantegazza M. Structural characterization of Ti centres in Ti-silicalite and reaction mechanisms in cyclohexanone ammoximation. *Catal Today.* 1996;32:97-106.

43 Jorda E, Tuel A, Teissier R, Kervennal J. TiF_4: An original and very interesting

precursor to the synthesis of titanium containing silicalite-1. *Zeolites.* 1997;19:238-245.

44 Zuo Y, Liu M, Zhang T, Hong L, Guo X, Song C, Chen Y, Zhu P, Jaye C, Fischer D. Role of pentahedrally coordinated titanium in titanium silicalite-1 in propene epoxidation. *RSC Adv.* 2015;5:17897-17904.

45 Li Q, Zhang Y, Chen G, Fan J, Lan H, Yang Y. Ultra-low-gold loading Au/CeO_2 catalysts for ambient temperature CO oxidation: Effect of preparation conditions on surface composition and activity. *J Catal.* 2010;273:167-176.

46 Lee SJ, Gavriilidis A. Supported Au catalysts for low-temperature CO oxidation prepared by impregnation. *J Catal.* 2002;206:305-313.

47 Kou J, Zhou X, Lu H, Wu F, Fan J. Graphyne as the membrane for water desalination. *Nanoscale.* 2014;6:1865-1870.

48 Bibby D, Milestone N, Patterson J, Aldridge L. Coke formation in zeolite ZSM-5. *J Catal.* 1986;97:493-502.

49 Sotelo JL, Uguina MA, Valverde JL, Serrano DP. Deactivation of toluene alkylation with methanol over magnesium-modified ZSM-5 shape selectivity changes induced by coke formation. *Appl Catal A Gen.* 1994;114:273-285.

50 Chen D, Rebo H, Moljord K, Holmen A. Effect of coke deposition on transport and adsorption in zeolites studied by a new microbalance reactor. *Chem Eng Sci.* 1996;51:2687-2692.

51 Mizuno N, Modern heterogeneous oxidation catalysis, New York: John Wiley & Sons, Inc., 2009.

52 Zhan G, Du M, Sun D, Huang J, Yang X, Ma Y, Ibrahim A-R, Li Q. Vapor-phase propylene epoxidation with H_2/O_2 over bioreduction Au/TS-1 catalysts: Synthesis, characterization, and optimization. *Ind Eng Chem Res.* 2011;50:9019-9026.

Figure captions:

Figure 1 In-situ UV-vis spectra of Au solution at different pH and at different charging sequences.

Figure 2 XRD patterns of titanium silicate-1 and silicate-1 samples (a) and nitrogen adsorption-desorption isotherms of TS-1 sample (b). The inset in Figure 2b shows the NL-DFT pore size distributions of TS-1.

Figure 3 FT-IR spectrum (a) and UV-vis spectrum (b) of TS-1.

Figure 4 Representative HAADF-STEM images and particle size distributions of the used Au/TS-1-SA (a, b), Au/TS-1-SB (c, d) and Au/TS-1-SC catalysts (e, f) at 200 ^{o}C. The scale bars represent 20 nm.

Figure 5 Selectivity (a) and PO formation rate (b) of Au/TS-1 catalysts prepared with different charging sequences.

Figure 6 Schematic diagram of the effect of charging sequence on Au locations and catalytic performances of Au/TS-1 catalysts.

Figure 7 Schematic diagram of pore filling and pore blocking mechanism (a) and V_c/V_{na} of the used 0.10 wt% Au/TS-1-SA and Au/TS-1-SB catalysts at different time-on-streams (b). The insets in Figure 7b shows the possible distribution of carbonaceous deposits.

Figure 8 PO formation rate of Au/TS-1-SA and Au/TS-1-SB catalysts as a function of time-on-stream.

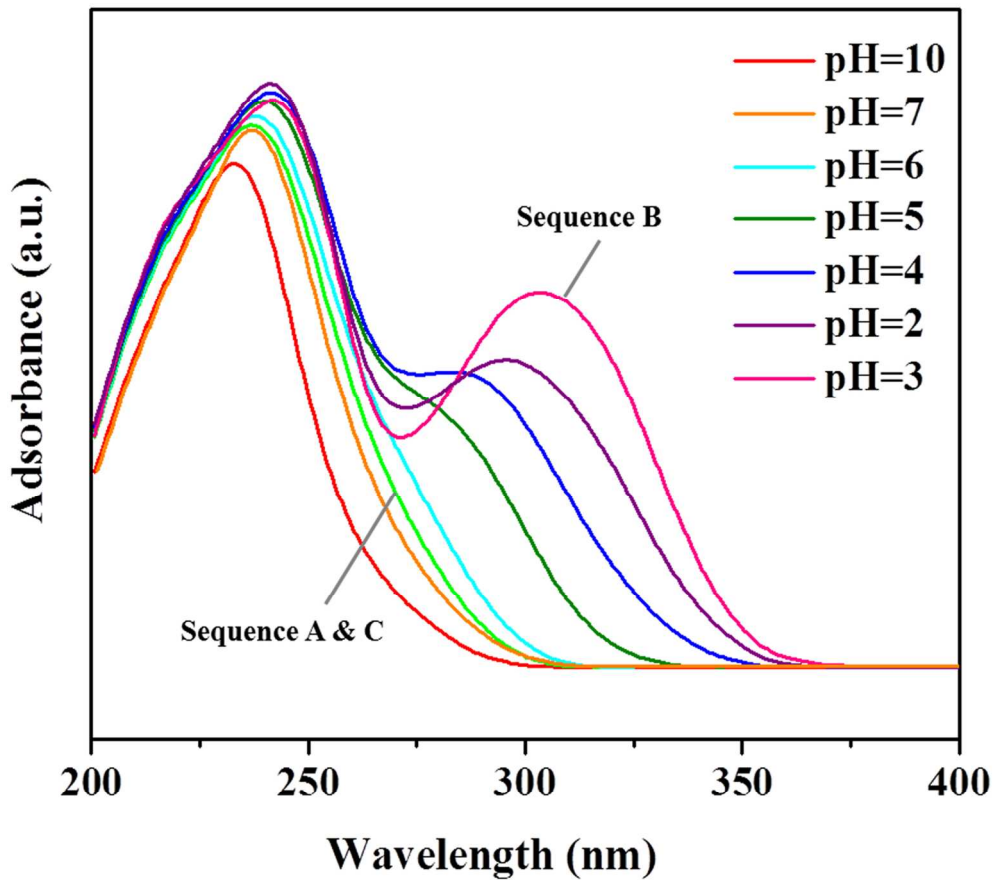

Figure 1 In-situ UV-vis spectra of Au solution at different pH and at different charging sequences.
126x111mm (300 x 300 DPI)

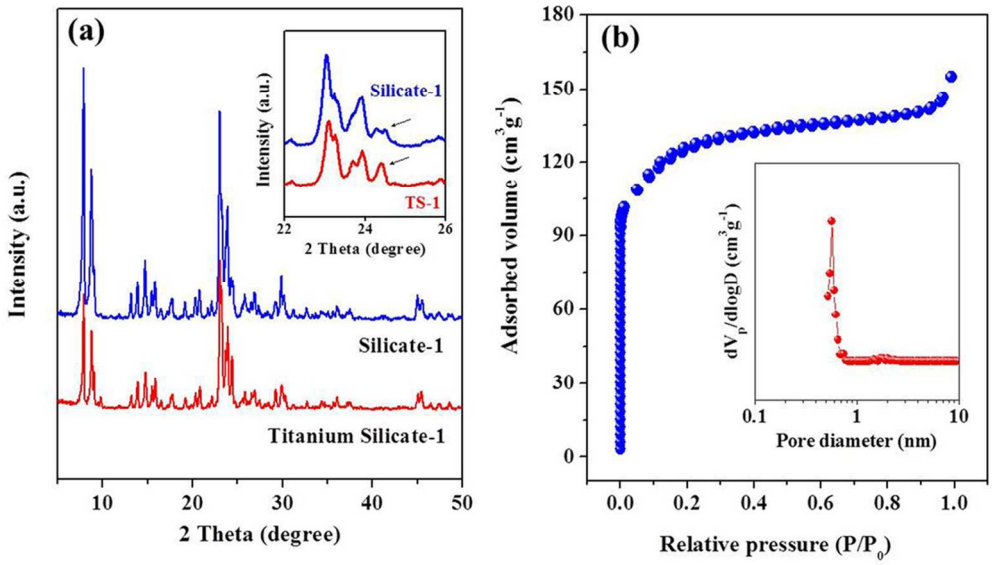

Figure 2 XRD patterns of titanium silicate-1 and silicate-1 samples (a) and nitrogen adsorption-desorption isotherms of TS-1 sample (b). The inset in Figure 2b shows the NL-DFT pore size distributions of TS-1.
114x65mm (300 x 300 DPI)

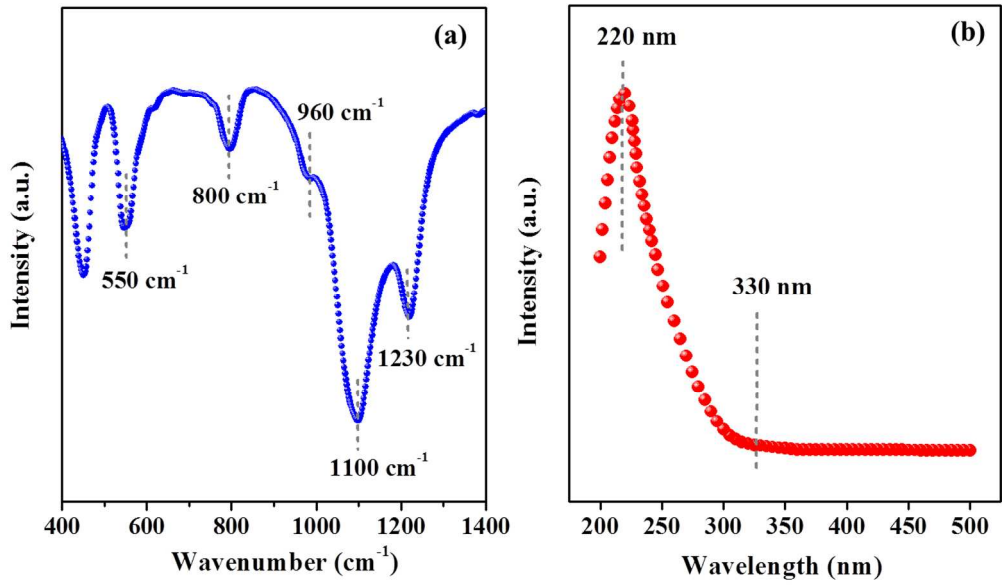

Figure 3 FT-IR spectrum (a) and UV-vis spectrum (b) of TS-1.
226x133mm (300 x 300 DPI)

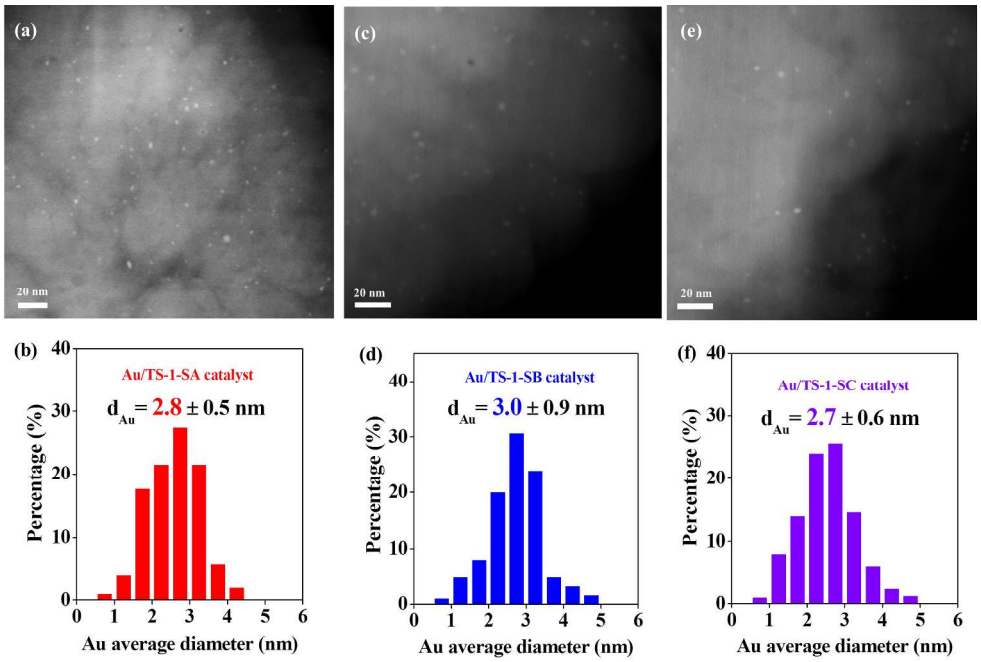

Figure 4 Representative HAADF-STEM images and particle size distributions of the used Au/TS-1-SA (a, b), Au/TS-1-SB (c, d) and Au/TS-1-SC catalysts (e, f) at 200 oC. The scale bars represent 20 nm.
469x310mm (300 x 300 DPI)

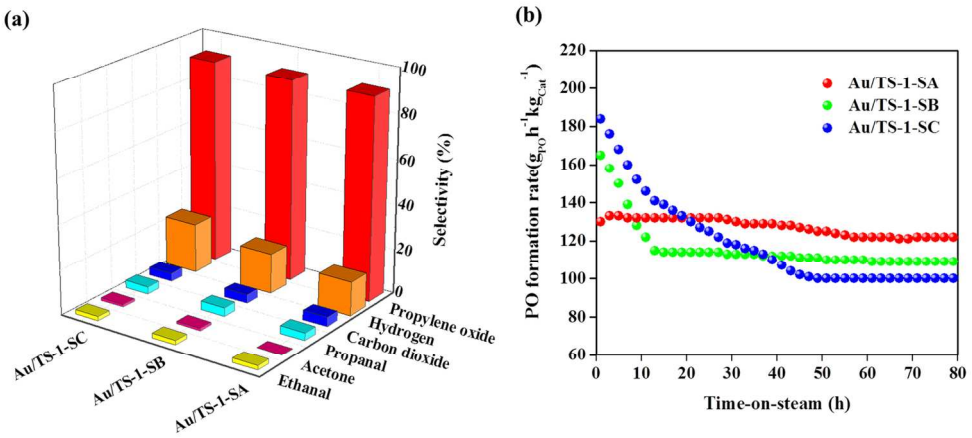

Figure 5 Selectivity (a) and PO formation rate (b) of Au/TS-1 catalysts prepared with different charging sequences.
146x66mm (300 x 300 DPI)

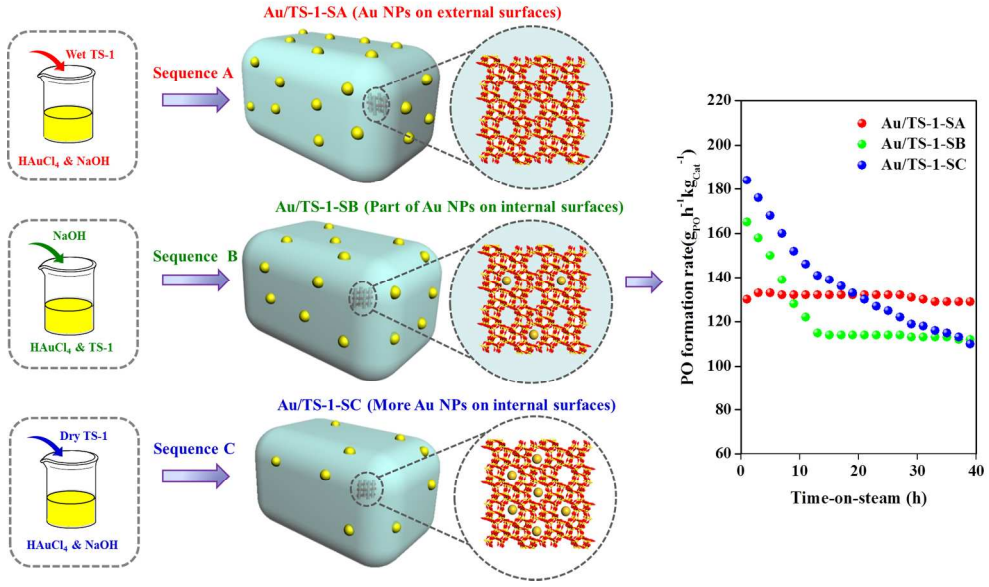

Figure 6 Schematic diagram of the effect of charging sequence on Au locations and catalytic performances of Au/TS-1 catalysts.
205x123mm (300 x 300 DPI)

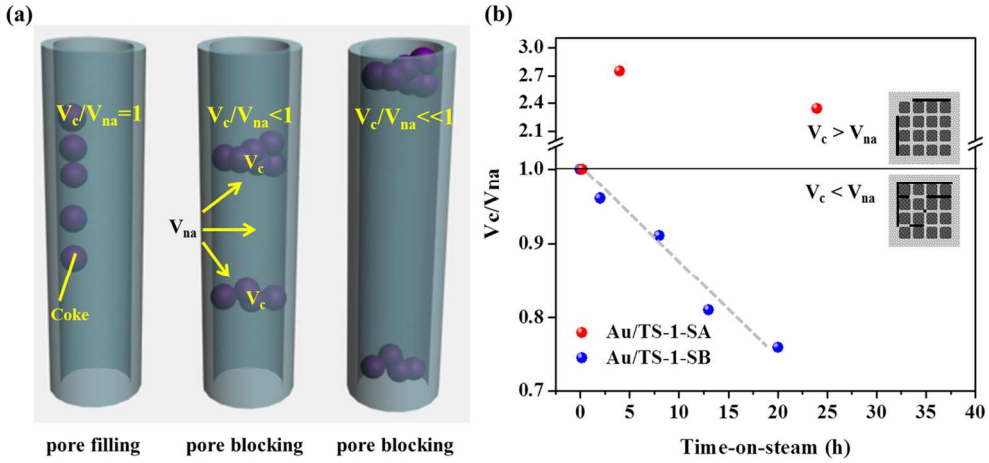

Figure 7 Schematic diagram of pore filling and pore blocking mechanism (a) and Vc/Vna of the used 0.10 wt% Au/TS-1-SA and Au/TS-1-SB catalysts at different time-on-streams (b). The insets in Figure 7b shows the possible distribution of carbonaceous deposits.
129x60mm (300 x 300 DPI)

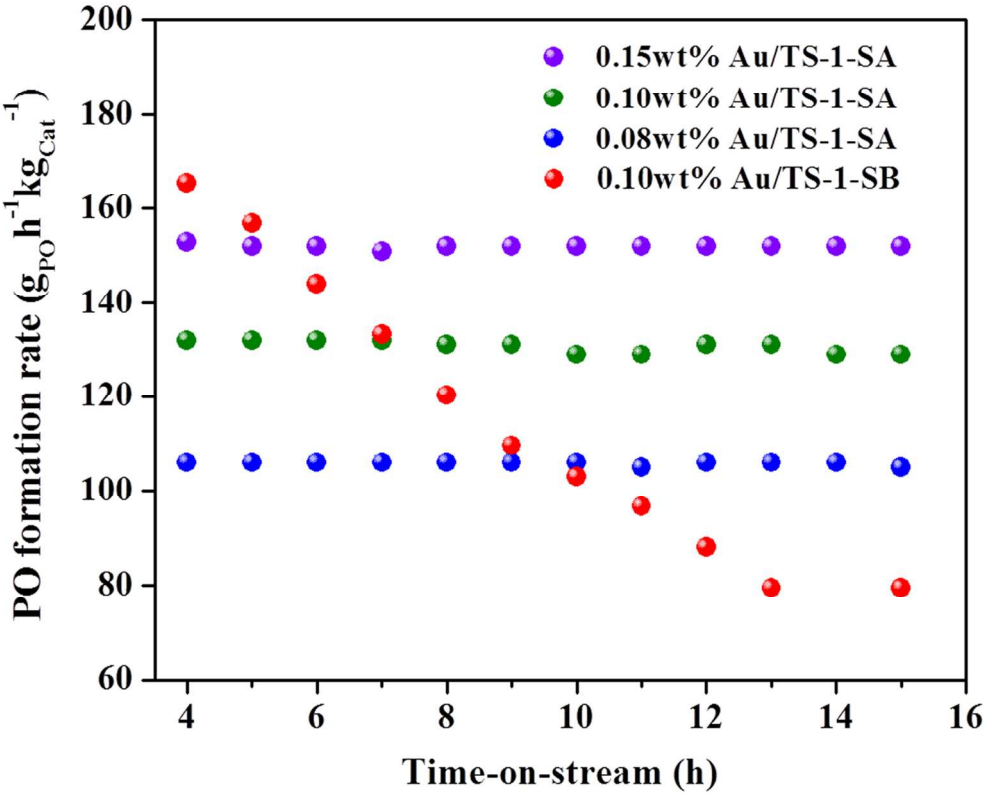

Figure 8 PO formation rate of Au/TS-1-SA catalysts as a function of time-on-stream.
131x105mm (300 x 300 DPI)

Table captions:

Table 1 The composition and size range of Au complexes at different charging sequences.

Table 2 The structural properties of TS-1 and Au/TS-1 catalysts prepared with different charging sequences.

Table 3 Surface and bulk compositions of Au/uncalcined TS-1 and Au/TS-1 samples prepared with different charging sequences.

Table 4 Properties of TS-1 support and Au/TS-1-SA catalyst at different time-on-steam.

Table 5 Catalytic performance of stable Au/Ti-containing catalysts.

Table 1 The composition and size range of Au complexes at different charging sequences.

Charging sequence	pH of Au solution when TS-1 is added	Existing Au complexes[a]	Size range of Au complexes[b] (nm)
Sequence A	7	$[AuCl_2(OH)_2]^-$, $[AuCl(OH)_3]^-$, $[Au(OH)_4]^-$	0.581-0.650
Sequence B	2-3	$[AuCl_4]^-$, $[AuCl_3(OH)]^-$	0.650-0.651
Sequence C	7	$[AuCl_2(OH)_2]^-$, $[AuCl(OH)_3]^-$, $[Au(OH)_4]^-$	0.581-0.650

[a] Existing Au complexes are determined according to the literature.[39]

[b] Size of Au complexes is determined by quench molecular dynamics in our previous work.[31]

Table 2 The structural properties of TS-1 and Au/TS-1 catalysts prepared with different charging sequences.

Sample	S_{BET} ($m^2 \cdot g^{-1}$)	V_{MP}[a] ($cm^3 \cdot g^{-1}$)	V_P[b] ($cm^3 \cdot g^{-1}$)	Reduced V_{MP}[c] ($cm^3 \cdot g^{-1}$)
TS-1	437	0.16	0.23	-
Au/TS-1-SA	440	0.16	0.23	0.00
Au/TS-1-SB	406	0.13	0.20	0.03
Au/TS-1-SC	393	0.11	0.19	0.05

[a] Micropore volume (V_{MP}) is estimated by t-plot method.

[b] Pore volume (V_P) is evaluated from the adsorption isotherm at the relative pressure about 0.99.

[c] Reduced micropore volume=$V_{MP(\text{TS-1 support})}$-$V_{MP(\text{Au/TS-1 catalyst})}$.

Table 3 Surface and bulk compositions of Au/uncalcined TS-1 and Au/TS-1 samples prepared with different charging sequences.

Sample	Actual Au loading (%)	Bulk Au/Si molar ratio (10^{-4})[a]	Surface Au/Si molar ratio(10^{-4})[b]
Au/uncalcined TS-1	0.10	-	41.6
Au/TS-1-SA	0.10	3.5	41.0
Au/TS-1-SB	0.10	3.4	5.2
Au/TS-1-SC	0.10	3.6	4.6

[a] Bulk Au/Si molar ratio is determined by AAS analysis.

[b] Surface Au/Si molar ratio is determined by XPS analysis.

Table 4 Properties of TS-1 support and Au/TS-1-SA catalyst at different time-on-steam.

Sample	S_{BET} (m^2g^{-1})	V_{MP}[a] (cm^3g^{-1})	wc[b]	V_c (10^{-2} cm^3g^{-1})	V_{na} (cm^3g^{-1})	V_c/V_{na}
TS-1	437	0.16	-	-	-	-
Au/TS-1-SA	440	0.16	0.00	0.00	0.00	1
Au/TS-1-SA-4h	436	0.15	3.30	2.75	0.01	2.75
Au/TS-1-SA-24h	393	0.14	5.60	4.67	0.02	2.34

[a] Au/TS-1-SA-*n* h represents Au/TS-1-SA catalyst from time-on-stream of n hours at 200 °C.

[b] Mass fraction of carbonaceous deposits (w_c) is determined by TGA.

[c] Micropore volume (V_{MP}) is estimated by t-plot method.

[d] Volume occupied by carbonaceous deposits (V_c) = w_c/ρ_c (the estimated density of carbonaceous deposits).

[e] Volume not accessible to N_2 (V_{na}) = V_{MP1}(fresh Au catalyst) $-V_{MP2}$ (used Au catalyst).

Table 5 Catalytic performance of stable Au/Ti-containing catalysts.

Catalyst	Preparation method	Si/Ti molar ratio	Au loading (wt%)	PO selectivity (%)	PO rate ($g_{PO}h^{-1}kg_{Cat}^{-1}$)	H_2 efficiency (%)
Au/TS-1[52]	SI	35	1.00	65*	75	25
Au/TS-1[3]	SG	36	0.10	90	50	28
Au/uncalcined TS-1[5]	DP	39	0.13	83	160	-
Au/TS-1-SA	DP	100	0.15	90	153	15

* The data from reaction temperature of 300 °C

Au/TS-1 Catalyst for Propene Epoxidation with H_2/O_2: A Novel Strategy to Enhance Stability by Tuning Charging Sequence

Xiang Feng[a], Yibin Liu[a], Yichuan Li[a], Zhihua Zhang[b], Xuezhi Duan[b], De Chen[c], Xinggui Zhou[b,*] and Chaohe Yang[a,*]

[a] *State Key Laboratory of Heavy Oil Processing, China University of Petroleum (East China), Qingdao 266580, China.*

[b] *State Key Laboratory of Chemical Engineering, East China University of Science and Technology, 130 Meilong Road, Shanghai 200237, China.*

[c] *Department of Chemical Engineering, Norwegian University of Science and Technology, Trondheim 7491, Norway.*

Abstract: For propene epoxidation with H_2 and O_2, the catalytic performance of Au/TS-1 catalyst is extremely sensitive to preparation parameters of deposition-precipitation (DP) method. In this work, effect of charging sequence in DP process on catalyst structure and catalytic performance of Au/TS-1 catalyst is first investigated. For different charging sequences, the compositions of Au complexes (e.g., $[AuCl(OH)_3]^-$) and pore property of TS-1 (i.e., with or without H_2O pre-filling micropores) could affect the transfer of Au complexes into the micropores, resulting in different Au locations and thus significantly different catalytic performance. Notably, when TS-1 is first filled with H_2O and then mixed with Au complexes, the reduced Au/TS-1 catalyst could expose Au nanoparticles on the external surface of TS-1 and show high stability. The results provide direct evidence showing that micropore blocking is the deactivation mechanism. Based on the results, a simple strategy to design highly stable Au/Ti-based catalysts is developed.

Keywords: Propene epoxidation, deposition-precipitation method, charging sequence, Au location, catalytic stability

*Corresponding author. E-mail address: xgzhou@ecust.edu.cn; yangch@upc.edu.cn

Introduction

Propylene oxide (PO) as a versatile chemical intermediate is used to synthesize derivatives such as polyurethane foams and propylene glycol. Traditional chlorohydrin and hydroperoxidation processes to produce PO usually suffer from environmental or economical problems. Since Haruta et al. reported an alternative process for PO production (i.e., direct propene epoxidation with H_2 and O_2) using Au/TiO_2 catalysts,[1] this environmentally benign, sustainable and simple process has attracted immense research interests.[2, 3]

For direct propene epoxidation with H_2 and O_2, the synergy between Au nanoparticles and isolated Ti^{4+}-containing supports is indispensable for PO formation.[4-7] This is because H_2O_2 synthesized by H_2 and O_2 on Au nanoparticles must transfer to isolated Ti^{4+} sites nearby and form Ti-OOH intermediate which entails the subsequent epoxidation of propene to PO. Therefore, measures have been taken to improve the Au-Ti synergy in the past decades.[5, 8-10] Deposition-precipitation (DP) method is most widely used to enhance this Au-Ti interaction because Au nanoparticles can be selectively deposited near active Ti^{4+} sites rather than Si^{4+} sites by adjusting the pH of Au solution higher than the isoelectric point of the inactive Si^{4+} sites. To date, a series of Au/Ti-containing catalysts (e.g., Au/uncalcined TS-1, Au/TS-1, Au/Ti-HMS, Au/Ti-TUD, Au/three-dimensional Ti-Si mesoporous zeolite, $Au/Ti\text{-}SiO_2$) prepared by DP method are efficient for propene epoxidation.[6, 7, 11-26] Among others, Au/TS-1 catalyst shows superior catalytic performance due to the unique physico-chemical properties of TS-1 support (e.g., abundant isolated Ti^{4+} species and high hydrophobicity).[7]

The catalytic activity of Au catalyst is reported to be significantly affected by the preparation parameters of DP method.[11, 25-29] For instance, Louis et al. reported that thorough washing could reduce the concentration of chlorine ions, leading to smaller Au particle size and higher catalytic performance.[30] Delgass et al. found that preparation temperature affects the Au loading efficiency and Au particle size.[26] Higher temperature results in the aggregation of Au species via condensation reaction, and thus the poorer PO formation rate. Lu et al. found that the pH of Au solution could also affect Au loading efficiency, and pH of 7 is more appropriate for PO formation.[28] Zhou et al. elucidated that the effect of aging time on the Au particle size distribution and the catalytic performance.[31] Although much attention has already been focused on the preparation parameters, the Au/TS-1 catalysts under similar preparation conditions still show significantly different Au atom efficiencies ($g_{PO}h^{-1}kg_{Au}^{-1}$).[27, 28, 32] Therefore, in-depth investigation on the effects of preparation parameters on physico-chemical properties and performance of Au catalysts are highly desired not only to the explanation of different catalytic behaviors but also to the rational design of more effective Au/Ti-containing catalysts for direct propene epoxidation.

Besides activity, the catalytic stability is another essential criterion for efficient Au catalysts. For traditional Au/Ti-containing catalysts prepared by DP method, one common issue is the fast deactivation. We proposed that the deactivation is mainly caused by micropore blocking, and then employed a special support (i.e., uncalcined TS-1 with TPA^+ template inside the micropores) to deposit Au nanoparticles on the external surfaces of TS-1.[5, 6, 7,31] The as-obtained Au/uncalcined TS-1 catalyst shows as expected high stability. However, this methodology to enhance the catalytic stability may not be extended to some Ti-containing supports because the chemical properties of templates are distinct. Therefore, there is an urgent need to develop a simple strategy to

improve the catalytic stability of Au/Ti-containing catalyst.

Herein, for the first time, the effect of charging sequence on catalytic structure and performance of Au/TS-1 catalyst for propene epoxidation with H_2 and O_2 is examined by multi-techniques such as in-situ UV-vis, HAADF-STEM, XPS, TGA and N_2 physisorption. It is revealed that the different compositions of Au complexes and pore structure of TS-1 (i.e., with or without water molecules inside the micropores) for each charging sequence greatly affect the mass transfer, i.e., the entrance of Au complexes in the micropores. This leads to different Au locations and catalytic performances. Notably, when the TS-1 support is first prefilled with water molecules and then mixed with Au complexes, the reduced Au/TS-1 catalyst has Au nanoparticles located on the external surfaces of TS-1. The as-obtained Au/TS-1 catalyst shows high stability, which is found to be due to the absence of micropore blocking phenomenon. Moreover, an efficient method derived from the deactivation mechanism is further developed to enhance the catalytic stability of Au/TS-1 catalyst from experimental and theoretical aspects. The insights in this work not only elucidate the effect of charging sequence on Au location and catalytic performance, but also provide an efficient scenario to enhance the catalytic stability of Au/Ti-containing catalyst for propene epoxidation. It is expected that this strategy could be extended to other supported metal catalysts to avoid the deactivation caused by micropore blocking phenomenon.

Experimental

Synthesis of TS-1 support and Au/TS-1 catalysts

Titanium silicalite-1 (TS-1) support was synthesized by traditional hydrothermal method according to previously reported synthesis procedure.[26, 33] In a typical procedure,

3.5 g polyoxyethylene 20-sorbitan monolaurate (Tween 20, Aldrich) was added to 50 mL deionized water at room temperature. Subsequently, a mixture of 66.4 g tetraethylorthosilicate (TEOS, 95 wt%) and 44.8 g tetrapropylammonium hydroxide (TPAOH, 25 wt%) was slowly added to the above solution under vigorously stirring. Afterwards, the required titanium (IV) tetrabutoxide (TBOT, 99 wt%) dissolved in 20 mL isopropanol (WAKO, 99.5 wt%) was added drop-wise to achieve Si/Ti molar ratio of 100. The resultant solution was then transferred to a Teflon autoclave and crystallized at 423 K for 48 h. The solid products were filtered and thoroughly washed with deionized water. Finally, the solid (i.e., uncalcined TS-1) is dried overnight and calcined at 823 K for 6 h. The as-obtained material is microporous TS-1.

Au/TS-1 catalysts with Au loading of 0.10wt% were prepared by the deposition-precipitation (DP) method with three different charging sequences as follows:

(1) Sequence A: 0.1 g $HAuCl_4 \cdot 3H_2O$ and 40 mL H_2O were mixed for 30 min. Meanwhile, 0.5 g TS-1 was added to 10 mL H_2O. The pH values of the two mixtures were adjusted to 7.3-7.5 by 1 M NaOH, respectively. Finally, the two mixtures were blended together and aged for ca. 9 h while the pH was maintained constant by adding a small amount of NaOH. The solid was then centrifuged for 30 min, washed twice with deionized water and dried at 28 ^{o}C under vacuum. The as-prepared catalyst is denoted as Au/TS-1-SA.

(2) Sequence B[5-7, 26, 27]: 0.5 g TS-1, 0.1 g $HAuCl_4 \cdot 3H_2O$ and 50 mL H_2O were mixed together and stirred for 30 min. Afterwards, the pH of the slurry was adjusted to 7.3-7.5 by 1 M NaOH and then aged for ca. 9 h. The as-synthesized solid was centrifuged, washed with deionized water and then dried under vacuum at room temperature. The

catalyst is denoted as Au/TS-1-SB.

(3) Sequence C[28, 34]: 0.1 g $HAuCl_4 \cdot 3H_2O$ and 50 mL H_2O were mixed for 30 min. The pH of Au solution was adjusted to 7.3-7.5 by 1 M NaOH. Subsequently, 0.5 g TS-1 was added to the above Au solution and the pH of Au slurry was maintained for ca. 9 h. The solid was then centrifuged for 30 min, washed twice with deionic water and dried at 28 ^oC under vacuum at room temperature. The as-synthesized catalyst is denoted as Au/TS-1-SC.

Catalyst characterization

The crystal phase of TS-1 was characterized by X-ray diffraction (XRD, Rigaku D/Max2550VB/PC, Cu K_α radiation). The micropore volumes of TS-1 and Au/TS-1 samples were measured by N_2 physisorption in a volumetric adsorption unit (Micromeritics ASAP 2020). The local environment of titanium (e.g., isolated Ti^{4+}, anatase TiO_2) was determined by diffuse reflectance ultraviolet-visable spectroscopy (DRUV-vis, Perkin Elmer Lambda 35) and fourier transform infrared spectroscopy (FT-IR, Nicolet 6700). The types of Au complexes at different charging sequence and different time were determined by in situ ultraviolet-visable spectroscopy on a spectrometer (in situ UV-vis, AvaSpec-2048) equipped with a transmission dip probe. The contents of carbonaceous deposits at different time-on-steam were analyzed by thermogravimetric analysis (TGA, Perkin Elmer TGA Pyris 1). The TGA analysis was performed by heating approximate 10 mg of dried sample from room temperature to 800^oC at a ramping rate 5^oC/min in a flow of N_2/O_2=8:1. The Au loadings were determined by atomic absorption spectroscopy (AAS, ZEEnit 600). The surface Au/Si molar ratios were analyzed by X-ray photoelectron spectroscopy (XPS) on a Kratos XSAM-800 instrument. Al K_α X-ray of 1486.6 eV is used as the excitation source. The

chloride ion concentration was examined by ion chromatography (Dionex 600). The average particle size and particle size distribution are determined by high-angle annular dark-field scanning transmission electron microscopy (HAADF-STEM) on a Tecnai G2 F20 S-Twin equipped with a digitally processed STEM imaging system. The Au particle size distribution was determined by measuring more than 150 nanoparticles.

Catalytic testing

Gas-phase propene epoxidation over Au/TS-1 catalysts was carried out at normal pressure in a feed gas mixture of C_3H_6: H_2: O_2: N_2 =1:1:1:7 at a space velocity of 14,000 $mLh^{-1}g_{cat}^{-1}$ under atmospheric pressure. 0.15 g catalyst of 60-80 mesh particle size was packed in a quartz tubular reactor (i.d. 8 mm). The reactor was heated from room temperature to 200 ^oC for reaction. The effluent was measured online by two gas chromatographs (Agilent 6890) equipped with TCD (Porapak Q and 5A columns) and FID (Porapak T column) detectors. The propene conversion, PO selectivity and H_2 selectivity were defined as follows:

Propylene conversion = mol of (C_3-oxygenates + 2/3ethanal + CO_2/3)/mol of propene in the feed.

PO selectivity = mol of PO/mol of (C_3-oxygenates + 2/3ethanal + CO_2/3).

H_2 selectivity = mole of PO/mol of H_2 converted.

Results and discussion

Effect of charging sequence

The charging sequence of deposition-precipitation process is easily overlooked. There is still no report on the effect of charging sequence on the physico-chemical structure of

catalyst and catalytic performance for propene epoxidation. It should be noted that when the charging sequence varies, the interaction between Au complexes and support may be different, which could result in different catalytic structure and performance.

The compositions of Au complexes for each charging sequence are investigated by UV-vis spectroscopy. Figure 1 shows the UV-vis spectrum of Au solution at different pH values. It can be seen that two adsorption bands ascribed to the ligand-to-metal charge transfer (LMCT) transitions from chlorine *p* to gold *d* orbitals are located at ca. 240 and 313 nm, which are associated with $p_\sigma \rightarrow d_{x^2-y^2}$ and $p_\pi \rightarrow d_{x^2-y^2}$ transitions, respectively.[35, 36] When the pH value is higher, the adsorption bands are blueshifted and the band intensities are gradually reduced. The reason for the change of bands is the hydrolysis of Au complexes, i.e., the gradual replacement of chloride by hydroxyl ions.[37] Table S1 shows the compositions of Au complexes at different pH values according to the literature.[38, 39] For example, the composition of Au complexes changes from $[AuCl_4]^-$ and $[AuCl_3(OH)]^-$ gradually to $[AuCl_2(OH)_2]^-$, $[AuCl(OH)_3]^-$ and $[Au(OH)_4]^-$ when the pH increases from 2 to 7. Based on the compositions of Au complexes at different pH values (Table S1) and the corresponding UV-vis spectra at different pH (Figure 1), it is therefore feasible to determine the compositions of Au complexes at each charging sequence from in-situ UV-vis spectra. Figure 1 also shows the in-situ UV-vis spectra of Au complexes for three charging sequences when TS-1 is mixed with Au solution. For charging sequence A and C, the pH of Au solution is already adjusted to 7.3-7.5 when TS-1 is added. There is only one adsorption band for Au/TS-1-SA and Au/TS-1-SC locating between the two bands at pH of 6 and 7. This indicates that the hydrolysis equilibrium is not reached and the composition of Au complexes should be $[AuCl_2(OH)_2]^-$, $[AuCl(OH)_3]^-$ and $[Au(OH)_4]^-$. For charging

sequence B, the pH value is still 2.3 when TS-1 is added, and the Au complexes are $[AuCl_4]^-$ and $[AuCl_3(OH)]^-$. The sizes of different Au complexes calculated by quench molecular dynamics[6] are shown in Table 1. It is clear that the size and steric hindrance of Au complexes with more chloride ions are larger. In addition, the sizes and steric hindrance of Au complexes for charging sequence B are larger than those for charging sequence A and C. Notably, the sizes of Au complexes are similar to the diameter of micropore, and Au complexes could enter into the micropores by stretching and bending vibrations but with difficulties.[31]

(Figure 1 should be inserted here)

(Table 1 should be inserted here)

TS-1 is employed as support to load the above Au complexes. Figure 2a shows the typical X-ray power diffraction pattern of TS-1 and the reference material of silicate-1. The two samples are high crystalline with the absence of an amorphous phase. It is clear that different diffraction peaks are located at $2\theta=7.9^o$, 8.8^o, 23.1^o, 23.9^o and 24.3^o, indicating the characteristic of MFI topological structure.[40] There is a single peak at $2\theta=24.3^o$ for TS-1, indicating the structure of orthorhombic unit cell symmetry.[26] This is obviously different from the two peaks at $2\theta=24.3^o$ for silicate-1, which is the characteristic of monoclinic unit cell symmetry. In addition, the peak ascribed to crystalline TiO_2 in the form of anatase at $2\theta=25.4^o$ is not observed for the TS-1 sample.[34] Figure 2b illustrates the nitrogen adsorption-desorption isotherms and pore size distribution of the TS-1 sample. According to the IUPAC classification, TS-1 exhibits typical type I isotherm with a steep rise at low relative pressure $P/P_0<0.01$, confirming the microporous character. The pore size distribution is determined by NL-DFT method, which shows accurate pore size distribution over the complete

micro/mesopore range. There is only a narrow peak centered at ca. 0.55 nm, fitting very well with the mean pore size of MFI structure.[7]

(Figure 2 should be inserted here)

Figure 3a shows the FT-IR spectrum of TS-1 sample. In accordance with XRD results, the MFI structure is certified by the band at 550 cm^{-1} which is assigned to the vibration of double five-membered ring unit.[31] The adsorption bands at 800 and 1100 cm^{-1} are attributed to the symmetrical and antisymmetrical stretching vibration of [SiO_4] units, respectively. In addition, the band at 1230 cm^{-1} is due to the asymmetrical stretching vibration of MFI framework structure. The peak at 960 cm^{-1} is often referred to Ti-O-Si band and is usually considered as a proof of Ti substitution into the framework.[41, 42] Figure 3b shows the UV-vis spectrum of TS-1. The dominant band centered at 210 nm is assigned to the $Ti^{4+}O^{2-}$ to $Ti^{3+}O^{-}$ ligand-to-metal charge transfer, and is characteristic of isolated tetrahedrally coordinated Ti atoms in framework.[43] No adsorption bands attributed to octahedrally coordinated Ti containing Ti-O-Ti bond or isolated Ti species coordinated water molecules[44] are observed at 240-290 nm. In addition, there is no adsorption band at 330 nm, indicating the absence of extra framework anatase TiO_2.[40] This is in consistant with the XRD results (Figure 2a).

(Figure 3 should be inserted here)

Table 2 shows the structural properties of TS-1 and Au/TS-1 samples. The micropore volume of pure TS-1 support is 0.16 $cm^3 \cdot g^{-1}$. After the deposition of Au clusters, the micropore volumes of Au/TS-1-SB and Au/TS-1-SC catalysts decrease from 0.16 to 0.13 and 0.11 $cm^3 \cdot g^{-1}$, respectively. The reduced micropore volume of Au/TS-1-SC catalyst (i.e., 0.05 $cm^3 \cdot g^{-1}$) is larger than that of Au/TS-1-SB catalyst (0.03

$cm^3 \cdot g^{-1}$), demonstrating that more Au clusters have entered into the microporous channels of TS-1. In contrast, the micropore volume of Au/TS-1-SA catalyst (0.16 $cm^3 \cdot g^{-1}$) is the same to that of pure TS-1 support. This indicates that Au nanoparticles do not enter the micropores but locate on the external surfaces of TS-1 for Au/TS-1-SA catalyst.

(Table 2 should be inserted here)

XPS is a powerful tool to analyze the surface composition of catalysts.[45] Table 3 shows the bulk and surface compositions of Au/uncalcined TS-1 and Au/TS-1 samples prepared with different charging sequences. The Au loadings of the four samples are carefully tuned to the same of 0.10 wt% in order to exclude the effect of Au loading on the XPS results. For the three Au/TS-1 catalysts, the bulk Au/Si molar ratios are quite similar due to the same Au loading. The surface Au/Si molar ratios are larger than bulk Au/Si molar ratios, confirming that Au nanoparticles tend to locate on the external surfaces of TS-1 rather than homogeneously distributed in the entire TS-1 volume.[11] In addition, the surface Au/Si molar ratios decrease in order of Au/TS-1-SA> Au/TS-1-SB> Au/TS-1-SC. This trend shows that more Au clusters are located inside the micropores for Au/TS-1-SC catalyst, in accordance with the N_2 physisorption results (i.e., minimum micropore volume of Au/TS-1-SC) in Table 2. Moreover, it can also be seen from Table 3 that the surface Au/Si molar ratios of Au/TS-1-SA and Au/uncalcined TS-1 catalysts are almost the same. For Au/uncalcined TS-1 catalyst, Au nanoparticles are deposited on the external surfaces of TS-1[7] because the TPA^+ template already blocks the micropores. This similar surface Au/Si molar ratios of Au/TS-1-SA and Au/uncalcined TS-1 catalysts corroborates that almost all the Au nanoparticles of Au/TS-1-SA catalyst are deposited on the external surfaces of microporous TS-1.

(Table 3 should be inserted here)

Figure 4 shows the typical HAADF-STEM images and particle size distributions of Au/TS-1 catalysts prepared with different charging sequences. The observable average Au particle size of the three samples are quite similar (Figure 4). However, the number of observable Au nanoparticles on the external surfaces of TS-1 decreases in order of Au/TS-1-SA> Au/TS-1-SB> Au/TS-1-SC. This tendency indicates that more Au nanoparticles are deposited on the external surface of TS-1 for Au/TS-1-SA catalyst while more Au clusters are located inside the micropores of Au/TS-1-SC catalyst. This indirect evidence is also in accordance with N_2 adsorption and XPS results.

(Figure 4 should be inserted here)

The unique location of Au nanoparticles on external surfaces of Au/TS-1-SA catalyst can be explained by the work of Gavriilidis.[46] They reported that when the support is dry, the solution can fill the pores of support and initially convective transport takes place.[46] However, when the support is wet with pure H_2O molecules (ca. 0.5 nm[47]) filling the pores, no convective solute transport takes place in the pores. Therefore, there is no more chemical reaction between Au complexes and Ti-OH inside the micropores. Subsequently, the hydrolyzed Au complexes in the solution react with Ti-OH groups on the external surfaces and pore mouth of TS-1 support (i.e., interface between pure H_2O inside micropores and Au complexes outside micropores). The as-formed hydroxy-gold species in the pore mouth may suppress the further diffusion of Au complexes into the micropores. This may be the reason for the unique Au location on Au/TS-1-SA catalyst. With respect to the more Au complexes inside the micropores of Au/TS-1-SC than Au/TS-1-SA catalyst, it is mainly because the size and steric hindrance of Au complexes for Au/TS-1-SC is smaller than that of Au/TS-1-SA catalyst when TS-1 is charged

(Table 1).

Figure 5 shows the different catalytic performances of three Au/TS-1 catalysts. PO formation rate and selectivity were determined at time-on-steam of 1h at 200°C. The PO selectivity of the three catalysts are ca. 90% and the selectivity of side products such as acetone, ethanal, propanal, carbon dioxide are also similar. The hydrogen efficiency of the Au/TS-1-SC catalyst is 22%, slightly higher than that of Au/TS-1-SA (18%) and Au/TS-1-SB (15%) catalysts. The slightly higher hydrogen efficiency of the Au/TS-1-SC catalyst is mainly because it contains more tiny Au nanoparticles inside microporous channels of TS-1 support. This part of tiny Au nanoparticles usually exhibit higher H_2 efficiency due to smaller Au particle size.[6] The PO formation rate of the three catalysts are obviously different, as shown in figure 5b. The differences are not due to effect of chloride because the careful washing eliminates chloride ions, as evidenced by the results of ion chromatography (Table S2). For 0.10 wt% Au/TS-1-SC catalyst, the initial PO formation rate is 185 $g_{POh}^{-1}g_{Au}^{-1}$, which is the highest among the three catalysts. For 0.10 wt% Au/TS-1-SB catalyst, the initial PO formation is slightly smaller than that of Au/TS-1-SC catalyst. It is reported by Delgass et al. that Au clusters inside the micropores may serve as the dominant active sites.[25] This statement is also supported by our previous works.[5-7, 31] Therefore, the higher initial PO formation rate for Au/TS-1-SC catalyst than Au/TS-1-SB catalyst is mainly due to larger proportion of Au clusters inside micropores of TS-1. Compared with Au/TS-1-SB and Au/TS-1-SC catalysts, the initial PO formation rate of Au/TS-1-SA catalyst is smaller. This may be due to the absence of the contribution of small quantity of high active Au clusters inside micropores of TS-1. Although the initial catalytic activity of Au/TS-1-SA catalyst is slightly lower than that of Au/TS-1-SB and Au/TS-1-SC catalysts, it shows high stability and thus higher stable catalytic activity after 20 h. This finding is also in

consistent with our previous finding[31] that with less Au clusters inside micropores of TS-1 support, the Au/TS-1 catalyst shows higher stable activity. The effect of charging sequence on Au locations and catalytic performance is shown in Figure 6.

(Figure 5 should be inserted here)

(Figure 6 should be inserted here)

New method to improve the catalytic stability

Fast deactivation is one of the key factors hindering the industrialization of Au/Ti-based catalysts. The Au/TS-1-SB and Au/TS-1-SC catalysts all suffer from the severe deactivation although the catalytic activities are high (Figure 5). In our previous work, we deposited Au nanoparticles on the external surfaces of uncalcined TS-1 which has TPA^+ template inside the micropores. The designed Au/uncalcined TS-1 catalyst shows significantly enhanced stability because of the easy transfer of reactants and products on the external surfaces of TS-1. However, the enhanced stability may also be attributed to the presence of amine species. In other words, the contribution of amine species generated during external TPA^+ decomposition on catalytic stability cannot be excluded. Herein, the Au/TS-1-SA catalyst is employed to elucidate the origin of the enhanced stability because Au/TS-1-SA catalyst does not contain any TPA^+ template.

The origin of the different catalytic stabilities of Au/TS-1-SA and Au/TS-1-SB catalysts is investigated by analyzing the volume of carbonaceous deposits (V_c) and the volume not accessible to N_2 molecules (V_{na}).[48-50] This analysis could show the relationship between carbonaceous deposits and TS-1 support (i.e., pore blocking and pore filling, as illustrated in Figure 7a). When carbonaceous deposits only lead to micropore filling, V_c should be equal to V_{na} and thus V_c/V_{na}=1. In contrast, V_c should be

smaller than V_{na} when the carbonaceous deposits cause micropore blocking, and hence $V_c/V_{na}<1$. When the carbonaceous deposits mainly block the pore mouth, V_c should be much smaller than V_{na}. The V_c is calculated by dividing the weight of carbonaceous deposits (i.e., w_c) by density of carbonaceous deposits (i.e., ρ_c), which are determined by TGA and FT-IR, respectively. The density of carbonaceous deposits with aromatic character (Figure S1) is usually 1.2 g·cm^{-3}.[50] Figure 7b shows the V_c/V_{na} of Au/TS-1-SA and Au/TS-1-SB catalysts as a function of time-on-steam. The values of V_c and V_{na} for Au/TS-1-SA and Au/TS-1-SB catalysts are summarized in Table 4. The data of Au/TS-1-SA is taken from our previous work.[7] It can be seen that V_c/V_{na} of Au/TS-1-SA catalyst decreases sharply from 1.00 to 0.75 in 20 h, indicating that micropore blocking is the deactivation mechanism. However, with the increase of volume of carbonaceous deposits, the volume not accessible to N_2 molecules (V_{na}) is slightly unchanged for Au/TS-1-SA catalyst (Table 4). This may be because carbonaceous deposits formed near Au nanoparticles on the external surface of TS-1 do not greatly affect the micropore volume. Consequently, the increasing V_c and almost unchanged V_{na} leads to large V_c/V_{na} of ca. 2.5 (larger than 1.0). The results demonstrate that micropore blocking phenomenon on Au/TS-1-SB catalyst does not occur on Au/TS-1-SA catalyst. Besides micropore blocking, another deactivation mechanism for Au catalysts is usually the Au aggregation. However, obvious Au aggregation is not observed for Au/TS-1 catalysts in propene epoxidation, as shown in Figure S2. This is also supported by other researchers.[7, 20, 28] Therefore, the origin for the high stability of Au/TS-1-SA catalyst is the unique location of Au on the external surfaces of TS-1 and hence the absence of micropore blocking phenomenon. When micropore blocking occurs, it is thus difficult for reactants and products to transfer into and out of the micropores of Au/TS-1-SB, inhibiting the reaction on internal Au-Ti active sites. Nevertheless, the easy mass

transfer on the external surfaces of Au/TS-1-SA guarantees the smooth epoxidation reaction.

(Figure 7 should be inserted here)

(Table 4 should be inserted here)

Without the TPA template, it is also feasible to deposit Au nanoparticles on the externals surfaces of TS-1 by manipulating the charging sequence. Figure 8 shows the catalytic performance of a series of Au/TS-1 catalysts prepared with charging sequence A in the initial 15 h. It is clear that none of the Au catalysts show any sign of deactivation, indicating that depositing Au nanoparticles on the external surfaces of support could indeed enhance the stability due to better mass transfer. With the increase of Au loading, the PO formation rate monotonously increases from 105 to 153 $g_{PO}h^{-1}kg_{Cat}^{-1}$. It should be noted that the normalized reaction rate ($g_{PO}h^{-1}g_{Au}^{-1}$) of 0.15Au/TS-1-SA catalyst is slightly lower than that of 0.08Au/TS-1-SA catalyst due to larger Au average particle size. Synthesizing smaller Au nanoclusters with high loading should be an effective approach to further enhance the catalytic activity, which will be carried out in our future research.

(Figure 8 should be inserted here)

The PO formation rate of reported stable Au/Ti-based catalysts without adding promoters are summarized in Table 5. The four Au catalysts including Au/TS-1-SA in this work all show Au nanoparticles on the external surfaces of TS-1 supports. The first two Au catalysts prepared by sol-immobilization (SI) and solid-grinding (SG) methods are effective for PO production, especially when promoters (e.g., ionic liquid and

alkaline) are added.[3, 21] In comparison, the Au/uncalcined TS-1 and Au/TS-1-SA catalysts prepared by DP method show much higher catalytic performance. This is mainly because Au nanoparticles could be selectively deposited near the Ti^{4+} sites rather than Si^{4+} sites by tuning the pH of solution higher than isoelectric point of Si^{4+} sites, which enhances Au-Ti synergy. With respect to the PO selectivity, the Au/TS-1-SA catalyst in this work is better than Au/uncalcined TS-1 catalyst. This is possibly due to the smaller Au particle size (Figure 4). The optimized catalytic performance of Au/TS-1-SA catalyst (i.e., 153 $g_{PO}h^{-1}kg_{Cat}^{-1}$) is already comparable to that of ethylene epoxidation to ethylene oxide (i.e., 134 $g_{PO}h^{-1}kg_{Cat}^{-1}$) in commercial plants.[51] The H_2 efficiency of Au/TS-1-SA catalyst can be further improved by reducing Si/Ti molar ratio of support since lower Si/Ti ratio favors the capture of H_2O_2 by the titanium centers near Au nanoparticles, thus hindering the direct decomposition of H_2O_2 to H_2O.[5] For zeolite catalyzed reactions (e.g., direct propene epoxidation with H_2 and O_2), a phenomenon is that reactants and products may face severe diffusion limitations that often lead to rapid catalyst deactivation by coke formation which blocks the pores. For propene epoxidation, if microporous materials supported Au catalysts (e.g., Au/Ti-MWW, Au/Ti-β, Au/TS-2) suffer from deactivation by micropore blocking, this strategy to deposit Au nanoparticles on the external surfaces may provide a promising way to enhance catalytic stability.

(Table 5 should be inserted here)

Conclusions

In this work, the effects of charging sequence in DP process on the structure and catalytic performance of Au/TS-1 catalyst are first investigated. It is found that the

composition of Au complexes and pore structure of TS-1 support (i.e., with or without H_2O molecules pre-filling the micropores) could affect the ability of Au complexes transferring into the micropores of TS-1, and thus change Au locations on the internal or external surfaces of support after reduction. When dry TS-1 support is mixed with small-sized Au complexes, more Au complexes could enter into the microporous channels of TS-1, resulting in higher initial PO formation rate but fast deactivation caused by micropore blocking. However, when TS-1 is first filled with H_2O and then mixed with Au complexes, the Au complexes are located on the external surfaces of TS-1 support. Consequently, the catalyst shows greatly enhanced stability. The reason for the stability is the absence of micropore blocking phenomenon as evidenced by the large V_c/V_{na} of used Au/TS-1-SA catalyst. Moreover, based on this strategy to enhance the catalytic stability using the charging sequence A, the 0.15wt% Au/TS-1-SA catalyst shows not only good stability over 15 h but also high PO formation rate of 153 $g_{PO}h^{-1}kg_{Cat}^{-1}$. This strategy is of referential importance to the design of highly stable Au/Ti-based catalysts for propene epoxidation with H_2 and O_2. It is hoped that this method could also be employed to enhance catalytic stability of other industrial supported metal catalysts that suffers from micropore blocking deactivation.

Acknowledgments

This work is financially supported by the 111 Project of Ministry of Education of China (B08021), China Postdoctoral Science Foundation (2015M582160) and the Open Project of State Key Laboratory of Chemical Engineering (SKL-ChE-15C04).

References

1 Haruta M, Uphade BS, Tsubota S, Miyamoto A. Selective oxidation of propylene

over gold deposited on titanium-based oxides. *Res Chem Intermed.* 1998;24:329-336.

2 Hayashi T, Tanaka K, Haruta M. Selective Vapor-Phase Epoxidation of Propylene over Au/TiO_2 Catalysts in the Presence of Oxygen and Hydrogen. *J Catal.* 1998;178:566-575.

3 Huang J, Takei T, Akita T, Ohashi H, Haruta M. Gold clusters supported on alkaline treated TS-1 for highly efficient propene epoxidation with O_2 and H_2. *Appl Catal B Environ.* 2010;95:430-438.

4 Bravo-Suarez JJ, Bando KK, Lu J, Haruta M, Fujitani T, Oyama T. Transient technique for identification of true reaction intermediates: Hydroperoxide species in propylene epoxidation on gold/titanosilicate catalysts by X-ray absorption fine structure spectroscopy. *J Phys Chem C.* 2008;112:1115-1123.

5 Feng X, Duan X, Yang J, Qian G, Zhou X, Chen D, Yuan W. Au/uncalcined TS-1 catalysts for direct propene epoxidation with H_2 and O_2: Effects of Si/Ti molar ratio and Au loading. *Chem Eng J.* 2014;278:234-239.

6 Feng X, Duan X, Qian G, Zhou X, Chen D, Yuan W. Insights into size-dependent activity and active sites of Au nanoparticles supported on TS-1 for propene epoxidation with H_2 and O_2. *J Catal.* 2014;317:99-104.

7 Feng X, Duan X, Qian G, Zhou X, Chen D, Yuan W. Au nanoparticles deposited on the external surfaces of TS-1: Enhanced stability and activity for direct propylene epoxidation with H_2 and O_2. *Appl Catal B Environ.* 2014;150:396-401.

8 Chen J, Halin SJ, Pidko EA, Verhoeven M, Ferrandez DMP, Hensen EJ, Schouten JC, Nijhuis TA. Enhancement of catalyst performance in the direct propene epoxidation: A study into gold-titanium synergy. *ChemCatChem.* 2013;5:467-478.

9 Qi C, Huang J, Bao S, Su H, Akita T, Haruta M. Switching of reactions between hydrogenation and epoxidation of propene over Au/Ti-based oxides in the presence of H_2 and O_2. *J Catal.* 2011;281:12-20.

10 Lee WS, Zhang R, Akatay MC, Baertsch CD, Stach EA, Ribeiro FH, Delgass WN. Differences in catalytic sites for CO oxidation and propylene epoxidation on Au nanoparticles. *ACS Catal.* 2011;1:1327-1330.

11 Lee W-S, Cem Akatay M, Stach EA, Ribeiro FH, Delgass WN. Enhanced reaction rate for gas-phase epoxidation of propylene using H_2 and O_2 by Cs promotion of Au/TS-1. *J Catal.* 2013;308:98-113.

12 Xu L, Ren Y, Wu H, Liu Y, Wang Z, Zhang Y, Xu J, Peng H, Wu P. Core/shell-structured TS-1@mesoporous silica-supported Au nanoparticles for selective epoxidation of propylene with H_2 and O_2. *J Mater Chem.* 2011;21:10852-10858.

13 Yang H, Tang D, Lu X, Yuan Y. Superior performance of gold supported on titanium-containing hexagonal mesoporous molecular sieves for gas-phase epoxidation of propylene with use of H_2 and O_2. *J Phys Chem C.* 2009;113:8186-8193.

14 Lu J, Zhang X, Bravo-Suárez JJ, Bando KK, Fujitani T, Oyama ST. Direct

propylene epoxidation over barium-promoted Au/Ti-TUD catalysts with H_2 and O_2: Effect of Au particle size. *J Catal.* 2007;250:350-359.

15 Qian G, Yuan YH, Wu W, Zhou XG, Vapor phase propylene epoxidation kinetics, *Stud Surf Sci Catal*. 2006;159:333-336.

16 Yuan YH, Zhou XG, Wu W, Zhang YR, Yuan WK, Luo L. Propylene epoxidation in a microreactor with electric heating. *Catal Today.* 2005;105:544-550.

17 Sinha AK, Seelan S, Akita T, Tsubota S, Haruta M. Vapor phase propylene epoxidation over Au/Ti-MCM-41 catalysts prepared by different Ti incorporation modes. *Appl Catal A Gen.* 2003;240:243-252.

18 Uphade BS, Akita T, Nakamura T, Haruta M. Vapor-phase epoxidation of propene using H_2 and O_2 over Au/Ti-MCM-48. *J Catal.* 2002;209:331-340.

19 Mul G, Zwijnenburg A, van der Linden B, Makkee M, Moulijn JA. Stability and selectivity of Au/TiO_2 and $Au/TiO_2/SiO_2$ catalysts in propene epoxidation: An in Situ FT-IR Study. *J Catal.* 2001;201:128-137.

20 Nijhuis TA, Huizinga BJ, Makkee M, Moulijn JA. Direct epoxidation of propene using gold dispersed on TS-1 and other titanium-containing supports. *Ind Eng Chem Res.* 1999;38:884-891.

21 Du M, Zhan G, Yang X, Wang H, Lin W, Zhou Y, Zhu J, Lin L, Huang J, Sun D, Jia L, Li Q. Ionic liquid-enhanced immobilization of biosynthesized Au nanoparticles on TS-1 toward efficient catalysts for propylene epoxidation. *J Catal.*

2011;283:192-201.

22 Sinha AK, Seelan S, Tsubota S, Haruta M. A three-dimensional mesoporous titanosilicate support for gold nanoparticles: Vapor-phase epoxidation of propene with high conversion. *Angew Chem Int Ed.* 2004;43:1546-1548.

23 Lee W-S, Cem Akatay M, Stach EA, Ribeiro FH, Nicholas Delgass W. Gas-phase epoxidation of propylene in the presence of H_2 and O_2 over small gold ensembles in uncalcined TS-1. *J Catal.* 2014;313:104-112.

24 Chen J, Pidko EA, Ordomsky VV, Verhoeven T, Hensen EJ, Schouten JC, Nijhuis TA. How metallic is gold in the direct epoxidation of propene: an FTIR study. *Catal Sci Tech.* 2013;3:3042-3055.

25 Lee WS, Lai LC, Cem Akatay M, Stach EA, Ribeiro FH, Delgass WN. Probing the gold active sites in Au/TS-1 for gas-phase epoxidation of propylene in the presence of hydrogen and oxygen. *J Catal.* 2012;296:31-42.

26 Lee WS, Cem Akatay M, Stach EA, Ribeiro FH, Delgass WN. Reproducible preparation of Au/TS-1 with high reaction rate for gas phase epoxidation of propylene. *J Catal.* 2012;287:178-189.

27 Huang J, Lima E, Akita T, Guzmán A, Qi C, Takei T, Haruta M. Propene epoxidation with O_2 and H_2: Identification of the most active gold clusters. *J Catal.* 2011;278:8-15.

28 Lu J, Zhang X, Bravo-Suárez JJ, Fujitani T, Oyama ST. Effect of composition and

promoters in Au/TS-1 catalysts for direct propylene epoxidation using H_2 and O_2. *Catal Today.* 2009;147:186-195.

29 Taylor B, Lauterbach J, Delgass WN. Gas-phase epoxidation of propylene over small gold ensembles on TS-1. *Appl Catal A Gen.* 2005;291:188-198.

30 Hugon A, El Kolli N, Louis C. Advances in the preparation of supported gold catalysts: Mechanism of deposition, simplification of the procedures and relevance of the elimination of chlorine. *J Catal.* 2010;274:239-250.

31 Feng X, Duan X, Cheng H, Qian G, Chen D, Yuan W, Zhou X. Au/TS-1 catalyst prepared by deposition-precipitation method for propene epoxidation with H_2/O_2: Insights into the effects of slurry aging time and Si/Ti molar ratio. *J Catal.* 2015;325:128-135.

32 Liu T, Hacarlioglu P, Oyama ST, Luo MF, Pan XR, Lu JQ. Enhanced reactivity of direct propylene epoxidation with H_2 and O_2 over Ge-modified Au/TS-1 catalysts. *J Catal.* 2009;267:202-206.

33 Khomane RB, Kulkarni BD, Paraskar A, Sainkar SR. Synthesis, characterization and catalytic performance of titanium silicalite-1 prepared in micellar media. *Mater Chem Phys.* 2002;76:99-103.

34 Sanz R, Serrano D, Pizarro P, Moreno I. Hierarchical TS-1 zeolite synthesized from SiO_2-TiO_2 xerogels imprinted with silanized protozeolitic units. *Chem Eng J.* 2011;171:1428-1438.

35 Gangopadhayay AK, Chakravorty A. Charge transfer spectra of some gold (III) complexes. *J Chem Phys.* 2004;35:2206-2209.

36 Peck JA, Tait CD, Swanson BI, Brown Jr GE. Speciation of aqueous gold (III) chlorides from ultraviolet/visible absorption and Raman/resonance Raman spectroscopies. *Geochim Cosmochim AC.* 1991;55:671-676.

37 Baatz C, Decker N, Prüße U. New innovative gold catalysts prepared by an improved incipient wetness method. *J Catal.* 2008;258:165-169.

38 Moreau F, Bond GC. Preparation and reactivation of Au/TiO_2 catalysts. *Catal Today.* 2007;122:260-265.

39 Nechayev YA, Nikolenko N. Adsorption of gold (III) chloride complexes on alumina, silica and kaolin. *Geochem Int.* 1986;23:142-146.

40 Duprey E, Beaunier P, Springuel-Huet M-A, Bozon-Verduraz F, Fraissard J, Manoli J-M, Brégeault J-M. Characterization of catalysts based on titanium silicalite, TS-1, by physicochemical techniques. *J Catal.* 1997;165:22-32.

41 Tatsumi T, Jappar N. Ammoximation of cyclic ketones on TS-1 and amorphous SiO_2-TiO_2. *J Catal.* 1996;161:570-576.

42 Zecchina A, Bordiga S, Lamberti C, Ricchiardi G, Scarano D, Petrini G, Leofanti G, Mantegazza M. Structural characterization of Ti centres in Ti-silicalite and reaction mechanisms in cyclohexanone ammoximation. *Catal Today.* 1996;32:97-106.

43 Jorda E, Tuel A, Teissier R, Kervennal J. TiF_4: An original and very interesting

precursor to the synthesis of titanium containing silicalite-1. *Zeolites.* 1997;19:238-245.

44 Zuo Y, Liu M, Zhang T, Hong L, Guo X, Song C, Chen Y, Zhu P, Jaye C, Fischer D. Role of pentahedrally coordinated titanium in titanium silicalite-1 in propene epoxidation. *RSC Adv.* 2015;5:17897-17904.

45 Li Q, Zhang Y, Chen G, Fan J, Lan H, Yang Y. Ultra-low-gold loading Au/CeO_2 catalysts for ambient temperature CO oxidation: Effect of preparation conditions on surface composition and activity. *J Catal.* 2010;273:167-176.

46 Lee SJ, Gavriilidis A. Supported Au catalysts for low-temperature CO oxidation prepared by impregnation. *J Catal.* 2002;206:305-313.

47 Kou J, Zhou X, Lu H, Wu F, Fan J. Graphyne as the membrane for water desalination. *Nanoscale.* 2014;6:1865-1870.

48 Bibby D, Milestone N, Patterson J, Aldridge L. Coke formation in zeolite ZSM-5. *J Catal.* 1986;97:493-502.

49 Sotelo JL, Uguina MA, Valverde JL, Serrano DP. Deactivation of toluene alkylation with methanol over magnesium-modified ZSM-5 shape selectivity changes induced by coke formation. *Appl Catal A Gen.* 1994;114:273-285.

50 Chen D, Rebo H, Moljord K, Holmen A. Effect of coke deposition on transport and adsorption in zeolites studied by a new microbalance reactor. *Chem Eng Sci.* 1996;51:2687-2692.

51 Mizuno N, Modern heterogeneous oxidation catalysis, New York: John Wiley & Sons, Inc., 2009.

52 Zhan G, Du M, Sun D, Huang J, Yang X, Ma Y, Ibrahim A-R, Li Q. Vapor-phase propylene epoxidation with H_2/O_2 over bioreduction Au/TS-1 catalysts: Synthesis, characterization, and optimization. *Ind Eng Chem Res.* 2011;50:9019-9026.